A MULTIPROXY RECORD OF ASIAN MONSOON VARIATIONS DURING THE LAST 15,000 YEARS FROM PEIKU CO, TIBETAN PLATEAU

A THESIS

SUBMITTED TO THE FACULTY OF THE GRADUATE SCHOOL

OF THE UNIVERSITY OF MINNESOTA

BY

MIAO DU

IN PARTIAL FULFILLMENT OF THE REQUIREMENTS

FOR THE DEGREE OF

MASTER OF SCIENCE

DR. RICHARD RICKETTS AND DR. STEVE COLMAN

MAY 2012

ACKNOWLEDGEMENTS

First of all, I would like to thank my advisors Doug Ricketts and Steve Colman for their guidance, advice, and patience during the course of this project. This project could not be finished without their encouragements along the way. I would also like to thank Erik Brown for being on my committee and providing constructive suggestion on the XRF data interpretation. I thank Josef Werne for his help in organic chemical analysis and his feedbacks on the biomarker discussion.

Second, I owe my thanks to Sarah Grosshuesch for her detailed instructions in the lab, which made it possible to obtain the data. And I thank Koushik Dutta for his analytical assistance with the GC-C-IRMS data.

Special thanks to Yongsong Huang and Rafael Tarozo at Brown University for allowing me to work in the lab and helping with the analyses of the GDGTs. Thanks to Jonathan Holmes at University of Glasgow for his help with the radiocarbon dating. And I would like to thank Andrew Henderson for core collection in the field, which made this project possible.

I am also grateful to the support of National Science Foundation (Grant No. 0732701), which made this project possible.

Finally, I thank my parents and friends for their love and support.

ABSTRACT

Knowledge of Asian monsoon variations will help extend our understanding of global atmospheric circulation. Numerous studies on the Tibetan Plateau have demonstrated the great potential of lake sediment records as indicators of monsoon induced climatic changes during the Holocene.

This study focuses on a multi-proxy record from Peiku Co, including XRF elemental composition, carbon isotopes of biomarkers, and GDGT indicies ($TEX_{86,}$ BIT, MBT/CBT), providing a paleoenvironmental history of this region on the southern Tibetan Plateau.

The study shows that the climate of the Peiku basin transitioned to wetter conditions after 15 ka BP, but the wetter phase was followed by an arid event between 13 ka and 11.5 ka BP that likely correlated to the Younger Dryas. The early- to mid-Holocene climate was wetter, while drier climate prevailed after 6.7 ka BP. The climate of the late-Holocene returned to wetter conditions, probably due to stronger SW monsoons. The cold event at 8.2 ka BP and a widespread event at 4.2 ka BP could not be distinctively identified in all the proxy records from Peiku Co.

The application of the BIT index indicated a constantly high amount of soil organic matter input to the lake, which biased the mean annual lake surface temperature as reconstructed by TEX_{86}. Most Tibetan lakes are greatly influenced by riverine supply, resulting in high BIT values. Further study of the GDGT distribution in soil, water column and lake sediments are needed for a better regional calibration of lake surface temperature and air temperature.

TABLE OF CONTENTS

LIST OF FIGURES

LIST OF TABLES

1. INTRODUCTION

The Asian monsoon is one of the most important aspects of atmospheric circulation in the Earth's climate system. Monsoon variations can cause flooding and droughts that impact nearly half of the world's population (Morrill et al., 2006). In addition, the Asian monsoon may affect climate globally, through interactions with El Niño (e.g., Liu et al., 2002) and mid-latitude circulation (e.g. Wang et al., 2001). Therefore, understanding past variations in the Asian monsoon will help extend our knowledge of global atmospheric circulation, as well as provide insights into the underlying climate-forcing mechanisms. Although there are continuous records of variations in both the East Asian (e.g. Wang et al., 2005) and Indian (e.g. Gupta et al., 2003) monsoons extending back over the Holocene, these records are obtained mostly from marine sediments and therefore tell us little about changes in the temporal and spatial patterns in temperature and precipitation on land during the Holocene.

Due to its unique tectonic setting and geographical location, the Tibetan Plateau is an ideal site for investigating long-term climate changes on land. First, the Tibetan Plateau plays an important role in triggering and maintaining monsoon circulation between the Eurasian continent and the oceans. Second, the Tibetan Plateau is located in a region where climatic conditions are complicated by the boundary between the westerlies and the Asian monsoon system. The present-day limit of monsoon rainfall crosses the Tibetan Plateau, causing it to be extremely sensitive to fluctuations in the strength of the monsoon. Moreover, the environment of Tibet has been relatively undisturbed by anthropogenic activities compared to India and eastern China.

Lake sediments are one of the most important terrestrial archives of paleoenvironmental and paleoclimatic information (Mingram et al., 2004). Despite the fact that western China is relatively dry, lakes are abundant in this area. Studies on the Tibetan Plateau have demonstrated the great potential of lake sediment records as indicators of past climate change.

In this study, we use a sediment core from Peiku Co, a small lake located on the Tibetan Plateau, to reconstruct paleoclimate variability associated with the Asian Monsoon. The primary goals of this study are to: 1) quantify the response of the terrestrial ecosystem surrounding Peiku Co to changes in hydroclimate; 2) reconstruct air temperature and hydroclimate in the study area and complement other paleoenvironmental records from Tibetan lake sediments; and 3) test the applicability of GDGT indices as an independent temperature proxy on small lakes.

This thesis contains the following sections: geological setting, materials and methods, results, discussion, and conclusions. Section two contains background information. In it I will briefly describe the geological setting of the Tibetan Plateau and Peiku Co, followed by the climate history of this region based on the records from several Tibetan lakes. I will also present previous studies on Peiku Co. Section three includes a description of the fieldwork, the materials used and the lab methods for sample preparation. I will outline the initial processing of core PC07-1B including the subsampling of the core sediments. Then I will provide the detailed lab operating procedures used in biogeochemical analysis.

In section four, I will present the results of all the analyses on the core sediment, including TOC, the XRF analyses, the TEX_{86}-based temperature reconstruction, the

MBT/CBT-based air temperature record, and the $\delta^{13}C$ values of the fatty acids. In section five I will discuss my interpretation of the major trends in all of the climatic proxies and compare my results to records from other Tibetan paleoclimate archives.

Section six contains conclusions. I will summarize the major results of this study, including the Holocene climate reconstructions on the Tibetan Plateau, its implication for the Asian monsoon intensity, and the potential for application of the GDGT-based proxies and compound-specific isotopic analysis in this system.

2. BACKGROUND

2.1 Holocene climate of the Tibetan Plateau

The Tibetan Plateau, with an area of over 2.5 million km^2 and an average elevation of 4,500 meters above sea level (masl), is the largest and highest plateau on Earth. The high altitude is caused by the Eocene collision between the Indian and Asian plates (ca. 50 Ma) and their continued convergence. Southern Tibet reached its current elevation by ca. 15 Ma (Harris, 2006). The plateau is bounded by the Tarim and Qaidam basins to the north, the Himalaya to the south and west, and the Tanggula Mountains on the east. Owing to its unique location and physical features, the Tibetan Plateau has played an important role in global climatic and environmental changes, especially the evolution of monsoon

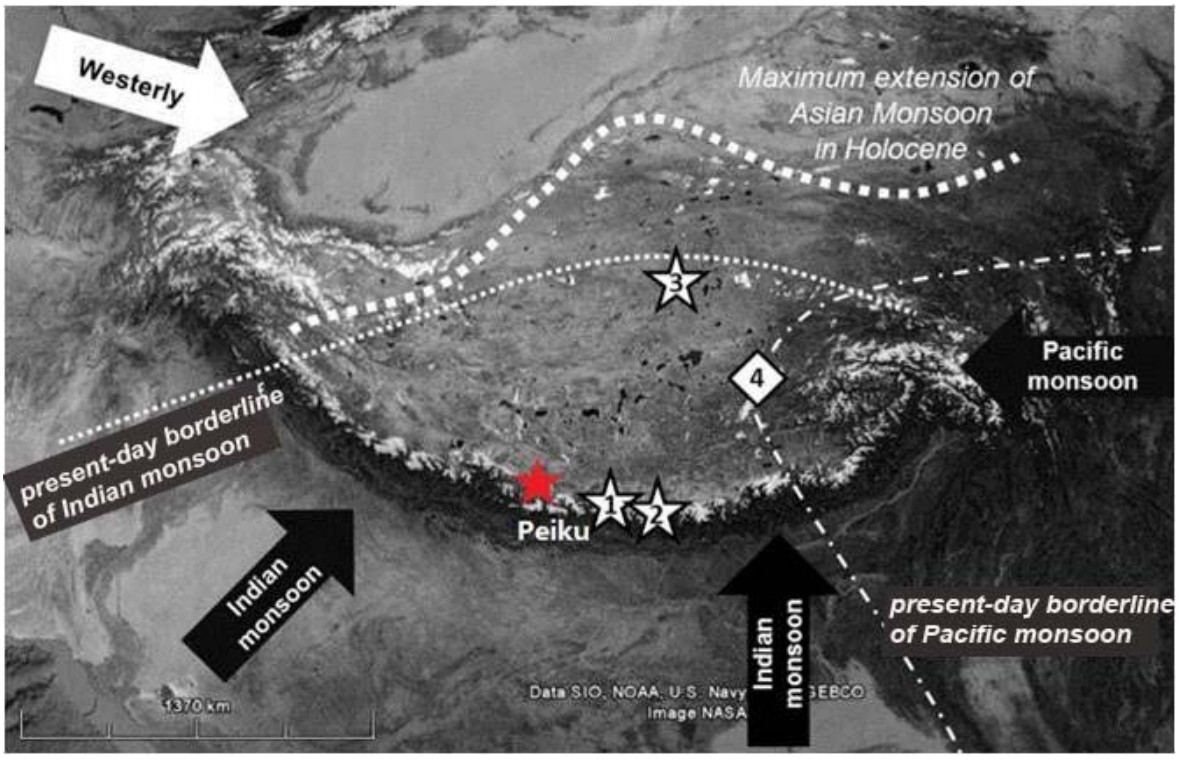

Figure 2.1.1 Controlling climate systems on the Tibetan Plateau. Red star marks the location of Peiku Co. 1-Dasuopu glacier, 2- East Rongbuk glacier, 3- Puruogangri ice cap 4. Nam Co (figure modified after Günther et al., 2011, original map source: Google Earth).

circulation since the Late Cenozoic (Ruddiman and Kutzbach, 1991; An et al., 2001).

The climate on the Tibetan Plateau is controlled by four interactive systems: the Westerlies, the East Asian monsoon, the Indian monsoon, and the Siberian cold polar airflow (Dong et al., 2010). The Indian monsoon is the dominant climate system impacting the southern Tibetan Plateau (Figure 2.1.1), the Indian subcontinent and most part of southwest China (Webster, 1994). The present-day limit of monsoon rainfall crosses the Tibetan Plateau, causing this region to be highly sensitive to monsoon variations. Therefore, paleoclimatic records from the Tibetan Plateau provide important clues for understanding the Asian monsoon system, which will extend our knowledge of the global atmospheric circulation and the underlying forcing mechanisms.

During the past two decades, a multitude of paleoclimate studies have been carried out in Tibet, with most of them focusing on lake sediments and ice cores in the northern, western and central Tibetan Plateau. Stable isotope records from Zabuye Salt Lake (western Tibet) indicate an arid-warm early and mid Holocene and a wet-warm Late Pleistocene (Wang et al., 2002), while sediment cores collected from Siling Co and Ahung Co (central Tibetan Plateau) both show increasing trends in temperature and precipitation during the early Holocene (10—8.4 ka BP), followed by the warmest and wettest period which occurred between 8.4—5.5 ka BP (Morinaga et al., 1993; Morrill, 2004). Multiproxy studies from Bangong Co and Sumxi Co (western Tibetan Plateau) indicate that lake levels were higher from 10 to 4 ka BP, especially between 9 ka and 5 ka BP (Gasse et al., 1991; Brown et al., 2003), and then lake levels begin to fall around 4 ka BP, which broadly agree with records from Siling Co and Lake Qinghai (Lister et al., 1991) at the eastern margin of the plateau. The $\delta^{18}O$ record from Guliya ice core suggests

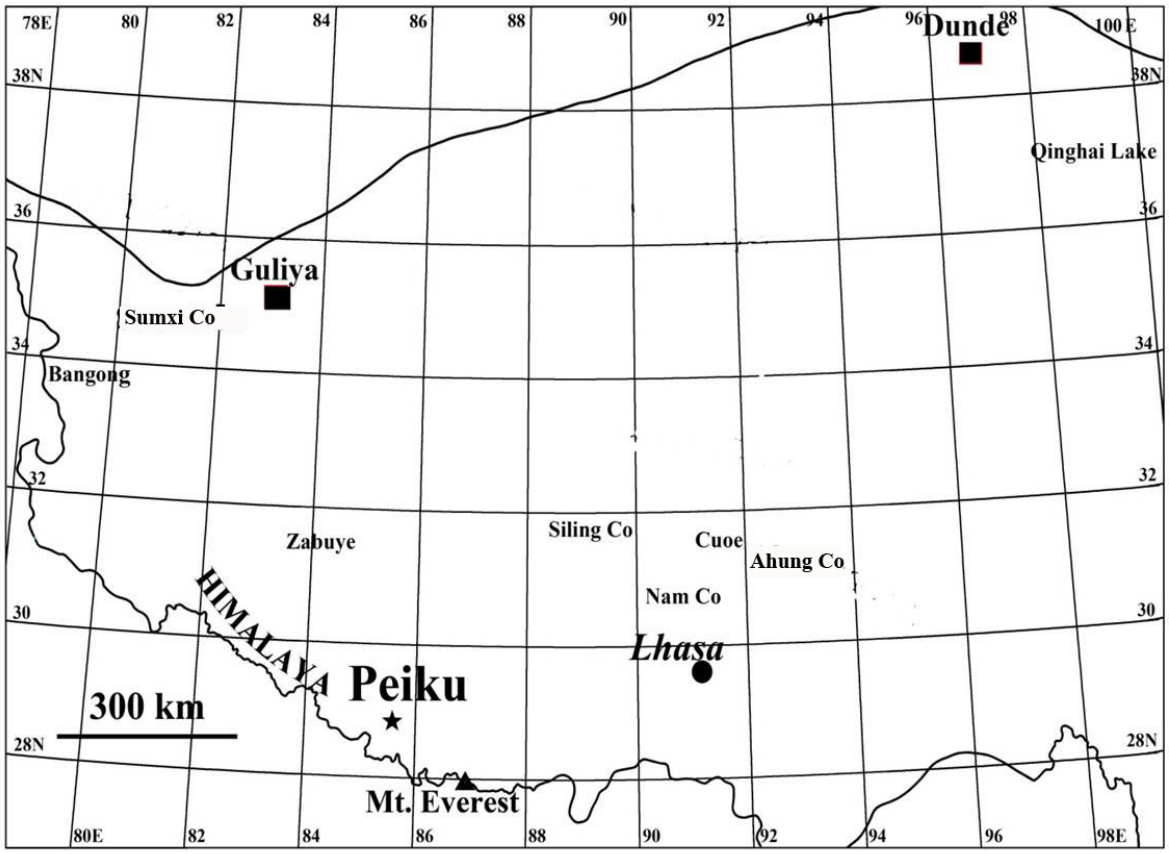

Figure 2.1.2 Locations of some Tibetan lakes and ice cores on the Tibetan Plateau. Solid back squares denote the location of ice core records. Others are names of lakes cited in the text.

that early Holocene temperatures rose from 10.5 to 9 ka BP and dropped between 9—8 ka BP (Thompson et al., 1997). The warmest period occurred between 7—6 ka BP, followed by a dramatic decrease in temperature around 5 ka BP. Unlike records from other study sites, the temperature at the Guliya ice core increased from 4—1.5 ka BP (Thompson et al., 1997; Yao et al., 1997). The pollen analysis from Dunde ice core shows a higher percentage of Artemisia with higher A/C ratio during 10—4.8 ka BP, suggesting a wetter climate in the northern Tibetan Plateau. Large variations in the Artemisia percentage and A/C ratio during 4.8—1.5 ka BP indicate dramatic climate

fluctuations (Liu et al., 1998). The δ^{18} O values from Dunde ice core indicate warmer climate conditions from 7.5—1.5 ka BP (Yao and Shi, 1992).

Considering the proxy resolution and age uncertainties in different records, the Holocene climate of northern Tibet began with a warm—wet period (10.5—5.4 ka BP), followed by a dry and most likely warm period (5—3 ka BP) and ended with a cool and dry stage (after 3 ka BP). The temporal and spatial patterns in climate change during the late Quaternary are still largely unknown in the southern Tibetan Plateau because of the lack of records. None of the records mentioned above are able to quantitatively reconstruct Holocene climatic changes due to uncertainties in chronology, low chronological resolution and incomplete understanding of the proxies preserved within the terrestrial archives.

2.2 Study area

Peiku Co (28° 50' N, 85° 35' E) is a brackish water lake situated in the southwestern Tibetan Plateau at 4595 masl (Fig. 2.1.2). The lake has a surface area of 280 km^2, and a maximum depth of 69 meters in the north basin (Fig. 2.2.1). Like many other lakes on the Tibetan Plateau, the basin of Peiku Co is of tectonic origin formed by faulting during the uplift of the plateau.

The Dingri weather station (28° 38'N, 87° 05' E, 4300 masl) records show that the mean annual temperature of this area is 0.7~2.7°C. The coldest month has an average temperature of -7 to -11 °C, while the warmest month has an average of 11-12°C. The precipitation in this region is mainly controlled by the southwest Asian monsoon. Mean annual precipitation at the weather station is around 200-300 mm. Peiku Co is located

150 km to the northeast of the Dingri weather station, so it is likely that Peiku Co has a lower temperature and less precipitation (Tibetan Plateau Expedition, CAS 1988). During the expedition in May, 2007, the water temperature was measured to be ~5°C throughout the water column, and the pH and salinity were also constant at ~8 and ~1.6‰, respectively (measured in May 2007, Henderson unpublished data).

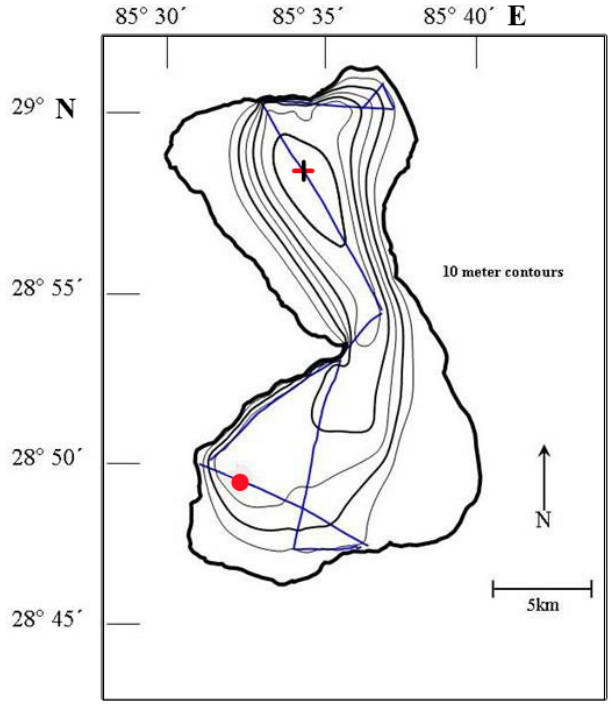

Figure 2.2.1 Bathymetry of Peiku Co. The blue lines are seismic tracklines. The red cross denotes the deepest point of the lake. The red circle is the core site of PC07-1B. (Ricketts, unpublished data)

The present-day vegetation around the lake is mainly classified as alpine steppe and alpine meadow. Due to the soil and hydrological conditions of the catchment, *Stipa purpurea* (monocots flowering plants) is the dominant species of vegetation in the area, together with other alpine species including *Artemisia* (sage), *Orinus thoroldii* (Stapf ex Hemsley) and *Pennisetum flaccidum* (flaccidgrass).

A previous study on spore-pollen samples collected from the third terrace on the south bank indicates that a cold-humid climate prevailed in this area between 13,000—10,760 a B.P., followed by a warm-humid period between 10,000—8,600 a B.P. Cold—dry conditions developed around 8,600—6,800 a B.P. and the climate became warmer between 6,800—5,000 a B.P.. High-resolution pollen analysis also suggests that three rainfall peaks occurred around 12,500, 10,000 and 6,000 a B.P. (Huang, 2000). Paleoenvironmental interpretations on ostracod assemblages (Peng, 1997) identified two cold events centered around 12,650—10,600 a B.P. and 6,730—6,500 a B.P., the latter most likely resulting from the major Holocene temperature decline. The cold pulse during 10,980—10,600 a B.P. could have been related to the Younger Dryas (Peng, 1997), which is seen in many records from northern and central Tibetan Plateau (Campo et al., 1993; Lister et al., 1991; Thompson et al., 1990). The transition from cold—dry climate to warm-wet conditions starts around 10,000 a B.P., which agrees with the pollen records in Peiku Co. However, these two studies failed to provide either the details about the dating methods or the age calibration.

2.3 Paleoclimatic proxies

2.3.1 Compound-specific carbon isotopes of molecular biomarkers

Bulk sedimentary $\delta^{13}C$ measurements are not sufficient to reconstruct vegetation changes because of the multiple sources of organic carbon with varied isotopic compositions delivered to lacustrine sediments (Meyers, 1997; Scholz et al., 2003). Compound-specific carbon isotopes of n-alkanes and n-alkanoic acids have been increasingly employed to examine the vegetation history and hydrological changes,

especially to infer source inputs and to elucidate palaeoenvironments of deposition (e.g., Freeman et al., 1990; Hayes et al., 1990).

The n-alkanes are straight long-chain hydrocarbons biosynthesized by terrestrial plants, aquatic plants, and certain algae (Eglinton and Hamilton, 1967). The carbon number distributions and isotopic compositions are dependent on the source organism. Terrestrial plants are characterized by strong odd-over-even predominance in the long-chain (C_{25}–C_{35}) carbon-numbered range (Rieley et al., 1991; Collister et al., 1994), while aquatic algae are dominated by the short-chain (C_{17}-C_{21}) n-alkanes (Giger et al., 1980). Likewise, n-alkanoic acids of terrestrial higher plants (leaf waxes) usually exhibit an even-over-odd predominance in the chain length of C_{26}-C_{32} (Eglinton and Hamilton, 1967), while shorter chain lengths are more likely to be influenced by microbial (algal and bacterial) contributions (Gong and Hollander, 1997; Meyers, 1997).

Not only are their carbon-number distributions indicative of their sources, but also the carbon isotopic compositions of biomarkers can serve as tracers for the photosynthetic pathways utilized by the vegetation. The $\delta^{13}C$ values of terrestrial biomarker molecules depend on that of the ambient atmospheric CO_2, the pathway employed during photosynthesis, e.g. whether it is the C_3 or C_4 pathway, and on factors (including aridity) that affect the conductance of the plant's stomata. Thus in turn, the carbon isotope composition reflects regional temperatures, aridity and pCO_2.

Generally, C_3 plants comprise most temperate species (~85%), including cold-season grasses, trees, shrubs, and herbs (Raven at al., 1999). They use the Calvin–Benson cycle characterized by the use of ribulose biphosphate carboxylase oxidase (RUBISCO). C_4 plants (~15%) are much less numerous and are typically tropical grasses and sedges, and

they use the Hatch-Slack cycle characterized by phosphoenol-pyruvate carboxylase (PEPC). RUBISCO has the largest kinetic isotope effect (~26%) between bulk plant tissue and CO_2 while the isotope effect of PEPC in C_4 plants (~5%) is much smaller (O'Leary, 1993; Lajtha and Marshall, 1994). Therefore, plants that follow the C_3 photosynthesis pathway have lower values of $\delta^{13}C$, between -22‰ and -30‰, while those following C_4 photosynthesis have higher values of $\delta^{13}C$, between -10‰ and –14‰ (Collister et al., 1994). A small number of plants, predominantly succulents, utilize a third photosynthetic pathway, the Crassulacean Acid Metablism (CAM) pathway, which could have $\delta^{13}C$ values between –10‰ and –30‰.

Further, C_3, C_4, CAM and aquatic plants also have different water-use efficiencies. C_4 plants have a better water-use efficiency because the pre-concentration mechanism of C_4 plants brings in CO_2 and keeps it in the cell with less leakage, so the plant does not need to keep its stomata open for as long (less water lost by transpiration) for the same amount of CO_2 for photosynthesis as the RUBISCO process. Accordingly, C_4 plants can cope better with lower atmospheric CO_2 conditions, higher temperatures and more arid habitats. The C_4 grasses dominate the huge areas of grassland and savannah which encircle the globe at sub-tropical latitudes in Africa, South America, parts of Australia and India (Still et al., 2003). These regions reflect the distribution of rain-deprived open environments which result from the impact of the prevailing patterns of the Earth's weather systems on the continents. Thus, assuming negligible contributions from CAM plants, one can use the $\delta^{13}C$ of long-chain leaf waxes in a given geographical area as a proxy for the relative proportion of C_3 and C_4 plants. In turn, these findings can reflect the climate parameters controlling them. The major factors controlling C_3 vs. C_4

vegetation change are believed to be temperature, aridity, and atmospheric CO_2 concentrations, however, the relative importance of the these factors is a topic of considerable debate (Cerling et al., 1997; Pagani et al., 1999; Huang et al., 2001). A study of five loess sequences across a large climatic gradient in the Chinese Loess Plateau indicates that East Asian summer monsoon intensity, which brings warmth and seasonal precipitation, is the dominant control of C_3 vs. C_4 vegetation changes in this region rather than atmospheric pCO_2 levels (Liu et al., 2005). Furthermore, the atmospheric pCO_2 levels have not changed considerably over the time period spanned in this study.

Compound-specific carbon isotopes of plant waxes have been applied as paleoclimate proxies in marine sediments (Hughen et al., 2004; Makou et al., 2007; Feakins et al., 2007; Huang et al., 2010; Galy et al., 2008 and 2011), and lacustrine sediments (Huang et al., 1999; Russell et al., 2009; Castañeda et al., 2009; Tieney et al., 2010); however, their use in continental China, where the Asian monsoons are the dominant control on temperature and precipitation, has only been applied to Chinese Loess sequences (Xie and Guo, 2004; Liu and Huang, 2005). One of the objectives of this study is to quantify the changes in the relative abundance of C_3 vs. C_4 plants based on the $\delta^{13}C$ from plant leaf waxes from lacustrine sediments on the Tibetan Plateau.

2.3.2 Glycerol Dialkyl Glycerol Tetraether (GDGT) lipids

One of the major challenges in paleoclimate reconstruction is to accurately determine temperature variability, for example the determination of past sea surface temperature (SST) changes during the last glacial maximum (Schouten et al., 2002). Although several

SST proxies have been developed during the last decades, such as the $\delta^{18}O$ and Mg/Ca ratios of planktonic foraminifera (Erez and Luz, 1983), and the U^{K}_{37}' ratio of long-chain unsaturated ketones (Brassell et al., 1986; Bard, 2001), the uncertainties in the source material and in the proxies' reliability back in time limit their applications. An independent temperature proxy based on lacustrine systems is needed to understand the global climate patterns and forcing mechanisms in the continents.

Glycerol dialkyl glycerol tetraethers (GDGTs) have in recent years become an interesting tool in paleotemperature reconstruction. The isoprenoid GDGTs (compounds I-V'; Figure 2.3.2) are membrane lipids derived from a ubiquitously occurring subgroup of archaea, the crenarchaeota. Recent studies proposed them to be reclassified to *Thaumarchaeota*, a separate phylum in the domain of archaea (Brochier-Armanet et al., 2008; Sprang et al., 2010). There is a strong correlation between mean annual SST and the relative abundance of cyclopentane-ring-containing GDGTs in the water column and surface sediments. Schouten et al. (2002) proposed an index called TEX_{86} (Tetraether indEX of tetraethers with 86 carbon atoms), which is based on the relative distribution of membrane lipids derived from marine thaumarchaeota, and is used for SST reconstructions. The TEX_{86} index is calculated as follows (Schouten et al., 2002)

$$TEX_{86} = \frac{[III] + [IV] + [V']}{[II] + [III] + [IV] + [V']} \qquad \text{Eq. 1}$$

The TEX_{86} index has been calibrated with a global set of core-top sediments from the world's oceans (Schouten et al., 2002, 2007; Kim et al., 2008).

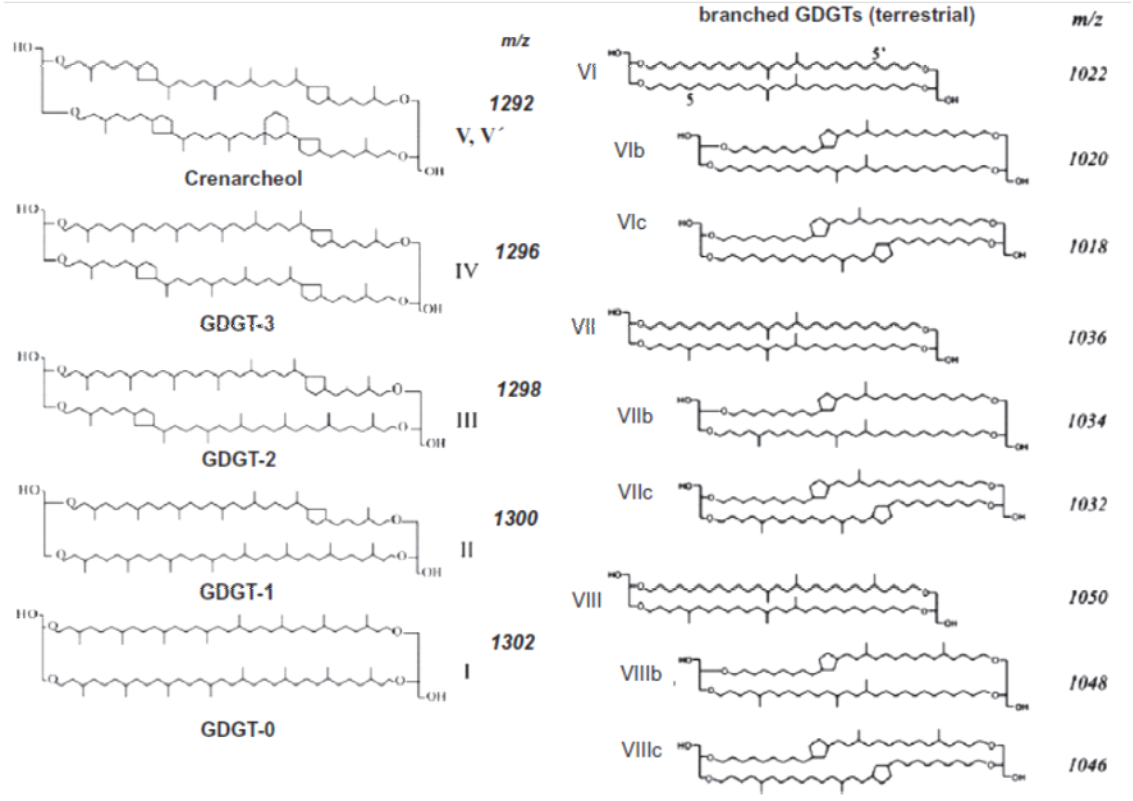

Figure 2.3.2 Isoprenoid and branched GDGT membrane lipids discussed in this paper (modified after Bechtel et al., 2004)

Generally, climate proxies established in the marine environment cannot be applied directly in lacustrine settings, but recent studies found comparable relationships between TEX_{86} and lake surface temperatures, indicating the applicability of the proxy as paleothermometer in at least some lacustrine systems (Powers et al., 2004; Tierney et al., 2007; Blaga et al., 2009).

Although it appeared successful initially, investigations of 48 globally distributed lakes suggest that the TEX_{86} paleotemperature proxy can be applied successfully only in a few, primarily large lake systems, while in small lakes its application is limited by several factors that affects the GDGT distribution (Powers et al., 2010). For instance, other archaea can biosynthesize some GDGTs that are identical to the ones produced by

the aquatic *Thaumarchaeota*, which may affect the distribution of sedimentary GDGTs and thus bias TEX_{86} values and the reconstructed temperatures (Weijers et al. 2006b). In addition, terrestrial input of archaeal membrane lipids may influence the GDGT distribution in lake sediments. The Branched and Isoprenoid Tetraether index (BIT; Hopmans et al. 2004) can be employed to estimate the input of allochthonous terrestrial GDGTS before calculating temperatures by means of TEX_{86} analysis. The BIT index is calculated using the equation proposed by Hopmans et al. (2004):

$$\mathrm{BIT} = \frac{[\mathrm{VI}] + [\mathrm{VII}] + [\mathrm{VIII}]}{[\mathrm{VI}] + [\mathrm{VII}] + [\mathrm{VIII}] + [\mathrm{V}]} \qquad \text{Eq. 2}$$

The BIT index ranges from 0, which indicates predominantly aquatic organic matter, to 1, which indicates predominantly soil derived organic matter. Therefore the BIT index can assess whether GDGTs used in TEX_{86} calculations are affected by the input of isoprenoid GDGTs from soil archaea.

A study of 47 lakes with various surface areas (1.1—5648 km^2) and characters along a south-north transect in Europe shows a variable distribution of GDGTs. The study suggests that GDGTs derived from thaumarchaeota are ubiquitous in lakes of all sizes throughout Europe (Blaga et al., 2009). To improve the applicability of TEX_{86} in lakes, a survey of core-top sediment GDGTs from 46 globally distributed lakes of varying size and diverse climate regions has been carried out (Powers et al., 2010). This study suggests that caution should be taken when applying TEX_{86} base temperature reconstruction in small lakes and that the BIT index should always be analyzed in concert with TEX_{86} analyses. The updated mean annual lake surface temperature (LST) is calculated following Powers et al. (2010):

$$\mathrm{LST}(°\mathrm{C}) = -14.0 + 55.2 * \mathrm{TEX}_{86} \quad \text{Eq. 3}$$

Eq. 3 was calibrated by removing eight lakes with BIT>0.5 to exclude potential biases of soil derived isoprenoid GDGT input. The linear relationship gives an estimated calibration error of ±3.7°C.

Another type of GDGT, the so called branched GDGTs (Figure 2.3.2 VI-VIII), have been attributed to soil bacteria (Hopmans et al., 2004). Weijers et al. (2007) suggested that the relative extent of cyclopentane moieties, expressed as the cyclisation ratio of branched tetraethers (CBT), is related to the pH of soil, while the relative extent of methyl branches, the methylation index of branched tetraethers (MBT) is positively related to mean annual air temperature (MAAT) and to some extent to soil pH. The MBT and CBT indices can be calculated as follows (Weijers et al., 2007):

$$\mathrm{MBT} = \frac{[\mathrm{VI}] + [\mathrm{VIb}] + [\mathrm{VIc}]}{[\mathrm{VI}] + [\mathrm{VIb}] + [\mathrm{VIc}] + [\mathrm{VII}] + [\mathrm{VIIb}] + [\mathrm{VIIc}] + [\mathrm{VIII}] + [\mathrm{VIIIb}] + [\mathrm{VIIIc}]} \quad \text{Eq. 4}$$

$$\mathrm{CBT} = -\log\frac{[\mathrm{VIb}] + [\mathrm{VIIb}]}{[\mathrm{VI}] + [\mathrm{VII}]} \quad \text{Eq. 5}$$

$$\mathrm{MBT} = 0.122 + 0.187 * \mathrm{CBT} + 0.02 * \mathrm{MAAT}\ (°\mathrm{C}) \quad \text{Eq. 6}$$

$$\mathrm{CBT} = 3.33 - 0.38 * \mathrm{pH} \quad \text{Eq. 7}$$

The MBT/CBT proxy has been applied to marine sediments from several areas and geological ages (Weijers et al., 2007a, 2007b; Schouten et al., 2008; Rueda et al., 2009). For example, based on the distribution of branched GDGTs in a sediment core from the Congo River fan, changes in the continental air temperature of tropical Africa over the last 25,000 yr could be reconstructed (Weijers et al., 2007a). The MBT/CBT reconstructed temperature for the Greenland land mass appeared to be in agreement with other air temperature reconstructions in this region (Schouten et al., 2008).

However, the MBT/CBT proxy has not been extensively studied in lacustrine systems (Tierney and Russell, 2009; Fawcett et al., 2011), and its applicability to high latitude environments with a maximum mean air temperature below 0℃ has not been totally confirmed, although a study on branched GDGTs in soils from Svalbard support the use of MBT/CBT proxy for terrestrial sites with a MAT < 0℃ (Peterse et al, 2009). Fawcett et al, (2011) has used this proxy to reconstruct the mean annual temperature in mid-Pleistocene lacustrine sediment from the Valles Caldera, New Mexico, with an estimated calibration error of ~2 ^{o}C. In a more recent study, the GDGT composition of 90 lakes, spanning a latitudinal gradient from the Scandinavian Arctic to the Antarctic Peninsula covering a wide temperature range (~1–31°C), was examined to constrain the MBT/CBT-derived temperature calibration. The new model with a root-mean-square temperature error of 2.0°C showed great potential for application to sediment cores to reconstruct past continental temperatures across a wide global area (Pearson et al., 2011).

In this study, we apply both of these GDGT-based temperature proxies in order to determine which, if either, is most appropriate for use in Peiku Co, and if possible, to reconstruct temperatures throughout the period of study in our core from Peiku Co.

3. MATERIALS AND METHODS

3.1 Sampling and Initial Core Description (ICD)

During an expedition in late spring 2007, three ~5-meter long sediment cores were collected using a UwiTek coring system, and three meter long surface sediment cores using a Glew corer. The core used in this study, PC07-1B, is a ~5.5 meter long core taken in 3 sections. Cores were retained in their original plastic liners and cut into ~150 cm segments in the field, sealed, and shipped back to the National Lacustrine Core Repository (LacCore) at the University of Minnesota, USA, for further analyses. The whole core was first logged on the Geotek Multisensor Core Logger track, which measures the sendiment density and loop-sensor magnetic susceptibility at 1 cm resolution. The core was subsequently split into working and archive halves. The archive half of the core was placed on the Geotek XYZ core scanner, which measured the high-resolution point-sensor magnetic susceptibility. The working half was imaged by a digital line scanner, which produces images at 10 pixels/mm. A color card was placed at each file for color correction, and the D-tube endcap was used in the picture for core identification.

3.2 Bulk Elemental Composition

The bulk element composition of PC07-1B was determined at the Large Lakes Observatory using the ITRAX X-ray Fluorescence Core Scanner (Cox Analytical Instruments). For relatively high mass elements such as iron, calcium, titanium, rubidium and strontium, the scanner was operated at a 2-mm resolution (corresponding to ~5 years) with a 60 second dwell time using a molybdenum X-ray source set to 30 kV and 20 mA.

For lower mass elements such as aluminum and silicon, the scanner was operated at a 2-mm resolution with a 30 second dwell time using a chromium X-ray source set to 30 kV and 20 mA.

3.3 Radiocarbon dating

Seven samples of bulk sedimentary material were collected for radiocarbon dating. The pre-treatment of raw samples was done at the Natural Environment Research Council (NERC, UK). The samples were digested in 2M HCl (80°C, 8 hours), washed free from mineral acid with deionized water then dried in a vacuum oven at 40°C. The total carbon in a known weight of the pre-treated sample was recovered as CO_2 by heating with CuO in a sealed quartz tube. The gas was converted to graphite by Fe/Zn reduction. Then the samples were sent to the Scottish Universities Environmental Research Center (SUERC) AMS Laboratory for ^{14}C analyses.

3.4 Total Carbon (TC), Total Inorganic Carbon (TIC) and Total Organic Carbon (TOC)

Fifty sediment samples were taken from PC07-1B at 10-20 cm intervals to be analyzed for total inorganic carbon (TIC) and total carbon (TC). The samples were freeze dried, powdered, and heated in an oven at 60°C overnight to remove any remaining water. A (20~30 mg) portion of each sample was then placed in a vial, weighed and the inorganic carbon was volatilized with 2N HCl in a CM 5130 acidification module. The released CO_2 was measured by an infrared detector using a UIC Inc. Coulometrics CM 5014 CO_2 coulometer. Another portion (20~30 mg) of each sample was placed into a small platinum boat which was then fired in a CM 5300 furnace apparatus at 950°C to

burn all the carbon present. This CO_2 also went to the coulometer and the amount was measured. The total organic carbon (TOC) could then be determined by subtracting the TIC from total carbon (TC). Two blanks were run before each batch of samples to make sure the instrument was adjusted to operating standard. A $CaCO_3$ standard was run after every tenth sample for evaluation of the instrumental accuracy, with acceptable results of 12% ± 0.5% total carbon. A duplicate was run every tenth sample as a quality check on reproducibility.

3.5 Lipid extraction and purification

Thirty samples were collected from core PC07-1B for organic geochemical analyses. About 5 g of dried and ground sediment samples were extracted via accelerated solvent extraction (ASE, DIONEX 350) with DCM:MeOH (9:1, v/v) mixture. The resulting total lipid extracts (TLE) were quantitatively split into two working halves. The first half of the TLE was methylated and then separated into different fractions through long silica gel column chromatogaphy including the n-alkanes, fatty acid methyl esters, alcohols, diols and GDGTs, and glycolipids. The n-alkane fractions were spiked with an internal standard (IS, 5α-androstane) for quantification on the Hewlett-Packard 6890 series II gas chromatograph (GC) using flame ionization detection (FID). The GC was equipped with a HP-1 column (30 m, 320 μm ID, 0.25 μm film thickness, Agilent). The oven was held at 50°C for 2 minutes and then raised to 325°C at 10°C/minute and held there for 10 minutes. The carrier (He) flow was constant at 2.6 ml/minute. The injection volume is 1 ml.

The other half of the TLE was separated into neutral, fatty acid and phospholipid bound fractions by eluting over Alltech aminopropyl bond elute columns. The fatty acid fractions (FAs) were methylated and then purified through short silica gel column chromatography. A method blank and a fatty acid standard (palmitic acid $C_{16}H_{32}O_2$) with known $\delta^{13}C$ values were methylated along with each batch of samples for further calibration. The fatty acid fractions were analyzed on a Hewlett-Packard 6890 series II gas chromatograph using flame ionization detection (FID). Quantification of compounds was performed by peak area integration in FID chromatograms relative to an internal standards 5α-androstane, which were added to sample vials prior to GC-FID injection. Each sample was analyzed in duplicate.

3.6 GDGT analyses

The GDGTs (Diols fraction) were analyzed at Brown University via high performance liquid chromatography/positive ion atmospheric pressure chemical ionization mass spectrometry (HPLC/APCI-MS), using selected ion monitoring mode (SIM), on an Agilent/Hewlett Packard 1200 series LC/MSD with an Alltech Prevail Cyano column (150x2.1mm, 3 μm). GDGTs were eluted isocratically for 5 minutes with 99% hexane:1% isopropanol, followed by a linear gradient to 1.8% isopropanol in 45 minutes. Flow rate was 0.2 mL per minute. TEX_{86} values were converted to temperature with the lakes-based calibration (Equation 3 above, Power et al., 2010).

3.7 Compound-specific carbon isotopic analyses

The $\delta^{13}C$ values of fatty acids (as FAMEs) were determined by gas chromatography-combustion-isotope ratio monitoring-mass spectrometry (GC-C-IRMS) with HP Agilent 6890N GC interfaced to a Thermo Finnigan Delta^{Plus} XP mass spectrometer, through a modified Thermo Combustion III unit at the Large Lakes Observatory. The GC oven temperature was increased at a constant rate of 3°C/minute from 100°C to 320°C. The $\delta^{13}C$ results were reported in conventional delta notation as per mil deviations from the VPDB standard. The $\delta^{13}C$ values were calibrated by analyzing standard mixtures of *n*-alkanes (Mix-A, C_{16}-C_{30}) and fatty acids (F-8, $C_{14:0}$-$C_{21:0}$) with certified $\delta^{13}C$ values for each component (standards provided by Prof. Arndt Schimmelmann, Dept. of Geology, Indiana University). A squalane standard ($\delta^{13}C$ = -20.49‰) was co-injected with the standards and the unknown samples for monitoring the reproducibility of the $\delta^{13}C$ measurements. Based on replicate measurements, typical precision of the $\delta^{13}C$ measurements were ±0.5‰ (1σ). A fatty acid standard (palmitic acid, $C_{16}H_{32}O_2$) of a known isotopic composition was used as a working reference standard for mass balance corrections for the added methyl group. All analyses were performed in duplicate.

4. RESULTS

4.1 Age-depth model

Initially, seven samples of bulk sedimentary material and one sample of wood were collected for radiocarbon dating. The samples were prepared to graphite at the NERC Radiocarbon Facility and sent to the SUERC AMS Laboratory for ^{14}C analysis. The eight ^{14}C ages were calibrated using the IntCal09.14 (Reimer et al., 2009) calibration curve and the midpoint values were used for age modeling (Table 4.1.1).

Table 4.1.1 Radiocarbon ages derived from accelerator mass spectrometry (AMS) of bulk organic matter (OMbulk) and a wood piece from core sediments from Peiku Co (PC07-1B). All dates are calibrated by Clam, using IntCal09.14 calibration curve. The age-depth model is established with midpoint values (^{14}C ages: Henderson, unpublished data).

Sample ID	Depth (cm)	Material	^{14}C Age (yrs BP)	Calibrated Age (2σ cal yrs BP)	Midpoint (cal yrs BP)	$\delta^{13}C$‰ (VPDB)
SUERC-23838	50	OMbulk	5410± 40	6295-6025	6270	-21.9
SUERC-23839	180	OMbulk	10220± 62	12207-10227	11850	-21.8
SUERC-23840	310	OMbulk	14450± 104	17917-17178	17601	-23.1
SUERC-23841	340	OMbulk	14400± 103	17888-17143	17567	-22.8
SUERC-23844	409	OMbulk	13900± 97	17364-16746	16945	-24.1
SUERC-23845	496	OMbulk	18700± 183	23203-21564	22320	-21.3
Poz-21140	496	Wood	Not available	14172-15052	14612	Not available
SUERC-23846	547	OM bulk	32300± 1051	39253-34744	36695	-21.2

The sample at 409 cm gives a date 13,900± 97 ^{14}C years, which was discarded due to an age reversal. Another sample dated 32,300± 1051 ^{14}C years was collected from the depth of 547 cm. This date was also excluded from the age-model because the date may not

accurately represent the age of the bottom lacustrine sediment. As mentioned in the initial core description, the sediment at depth 538-550 cm is composed of stiff and dense sand, which was likely deposited in shallow water and may have been partially eroded. The age-depth relationship is constrained by the five remaining calibrated ^{14}C dates. A linear interpolation provides a core-top (0 cm) age ~5000 cal yrs BP and bottom (538 cm) age ~24,903 cal yr BP (Figure 4.1.1).

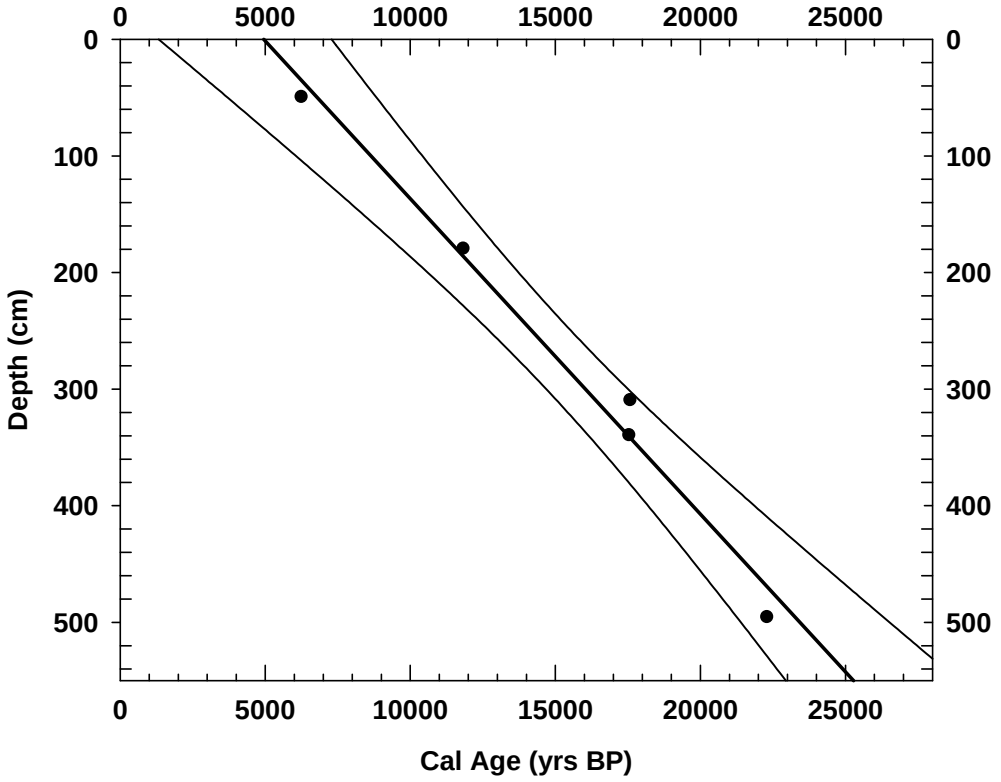

Figure 4.1.1 Age-depth relationship established on five calibrated radiocarbon dates with 95% confidence intervals. The linear interpolation $y = 0.0262x - 108.15$, $R^2 = 0.9812$

We suspect that there was some core over-penetration of the sediment column and that the uppermost part of the sediment column was not sampled by the corer. The linear interpolation outlined above estimates an over-penetration of ~110 cm. While this amount of core over-penetration is possible, there is also the possibility that the

radiocarbon ages of the lake sediment are influenced either by a strong reservoir effect or an old carbon effect (caused by terrestrial organic material bearing dead carbon derived from the catchment area or loess deposits). Such problems of radiocarbon dating on bulk organic matter are common in earlier studies of lacustrine sediments from the Tibetan Plateau (Fontes et al., 1996; Wang et al., 2002; He et al., 2004). ^{14}C analyses of terrestrial plant residues are preferable because direct fixation of atmospheric CO_2 occurs throughout the lifetime of plants (Watanabe et al., 2007). However, terrestrial plant remains are extremely rare in most Tibetan lake sediments due to the lack of vegetation in this area (Wang et al., 2002; Watanabe et al., 2008). The only wood sample found in Peiku Co sediment (at 496 cm depth) has an age of ~14,612 cal yrs BP. The offset between the calibrated age (~23,385 cal yrs BP) of the bulk sediment and wood samples at 496 cm is ~8,773 calendar years at this depth. The reservoir effect alone cannot explain this huge age gap since the maximum possible age error is equivalent to the half-life of ^{14}C, 5,570 yr (Libby scale). This implies that at least ~3,000 years of the age difference between the wood sample and the bulk organic matter is due to old carbon from the catchment being deposited in the lacustrine sediment. We cannot assume that the effect is the same throughout the whole core, because the physical and chemical conditions (e.g. water level, mixing) in the lake may have changed over time. As an accurate chronology is of crucial importance for the paleoenvironment study of Peiku Co, an alternative age model is established by comparing the $\delta^{18}O$ record of ostracod assemblages in Peiku Co with a high-resolution and independently dated oxygen isotope record from Dongge cave (Figure 4.1.2). The principle applied here assumes that proxy variations in different archives have been produced by major climate and environmental events of global scale,

and they were recorded in various types of deposits from multiple regions almost simultaneously (Maarten Blaauw, 2010). The Dongge Cave record provides a continuous Asian monsoon history over the last 16 ka from the $\delta^{18}O$ record of stalagmite calcite.

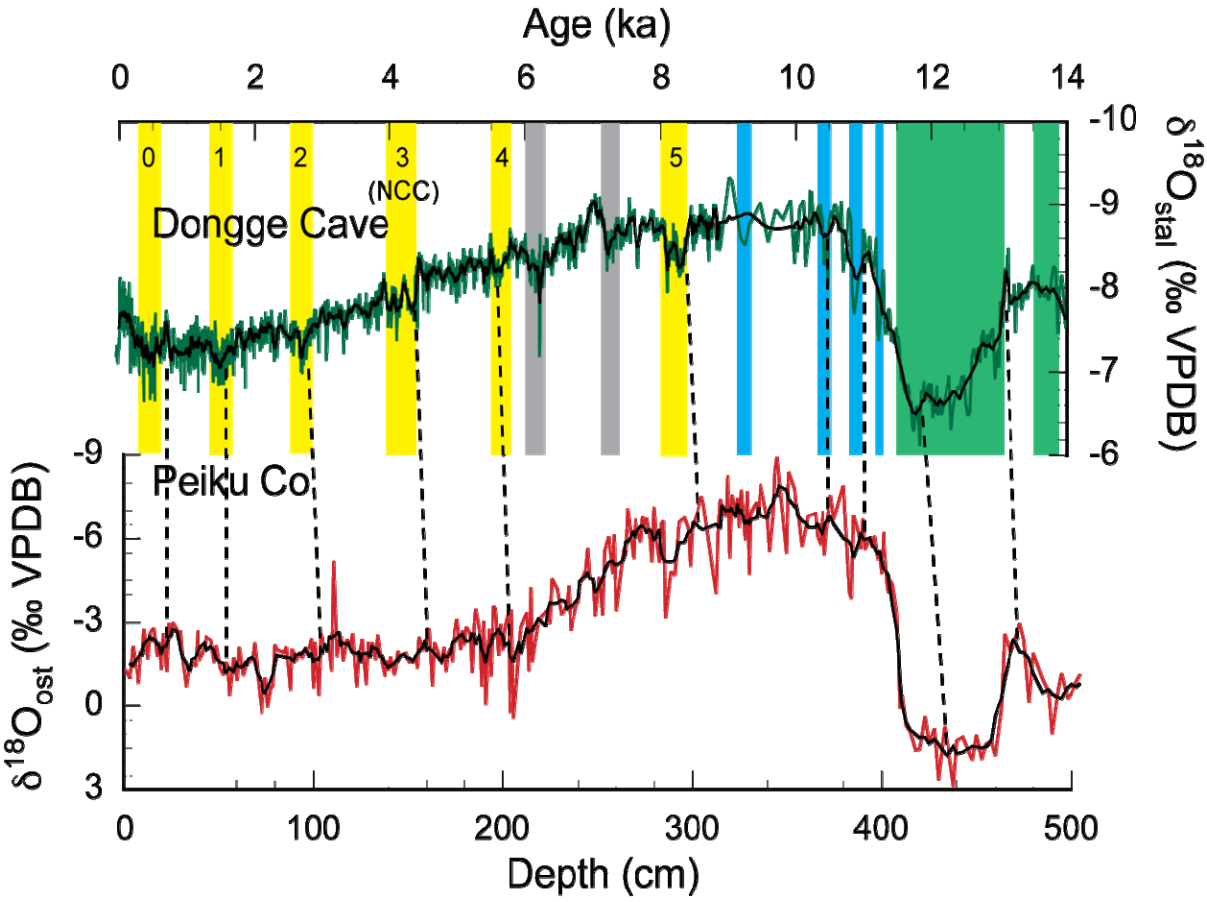

Figure 4.1.2 $\delta^{18}O$ record of stalagmite calcite from Dongge Cave, China (data taken from http://www.ncdc.noaa.gov/paleo/speleothem.html) and the $\delta^{18}O$ of ostracod assemblage from Peiku lake sediment (Andrew Henderson, personal communication) Dashed lines indicate the tie points used in Peiku

The chronology was constrained by 45 ^{230}Th dates and a linear interpolation was used to calculate an age for each of the 900 $\delta^{18}O$ samples. The $\delta^{18}O$ values began to rise at ~13 ka and by 12.5 ka had risen by 2‰ to heavier values, which corresponds to the beginning of the Younger Dryas as recorded in Greenland. At ~11.5 ka, the $\delta^{18}O$ values fell to lighter values of -8.4‰, within error of the end of the Younger Dryas (Dykoski et al.,

2005). A strong correlation can be seen in the ostracod record of Peiku Co (Henderson unpublished data, and Fig. 4.1.2) when aligning the two proxy curves. Assuming that these proxy events were registered synchronously in both records and the accumulation rate is constant, the ages of the sediments deposited during these $\delta^{18}O$ events in Peiku Co could be estimated (Table 4.1.2). An alternative age-depth model can therefore be built upon these tie-points by a linear interpolation (Figure 4.1.3). The resulting age model yields a core-top age of ~250 a BP and a bottom age around 15,000 a BP. The age at 496cm is 13,873 a BP from this model, resulting in an age offset of ~8,711 years, almost the same as that estimated from the original ^{14}C dates, which indicates this alternative model might provide a better age estimation than the original calibration.

Table 4.1.2 Estimated age points of Dongge Cave and the corresponding depths from Peiku Co.

Depth (cm) Lake Peiku	**^{230}Th Age (yrs BP) Dongge Cave**	**$\delta^{18}O$ (‰VPDB) Dongge Cave**
20	500±30	-7.7
30	1494±50	-7.5
100	2729±138	-6.9
150	4402±50	-8.3
200	5595±75	-8.4
300	8257±75	-8.3
370	10453±77	-8.6
390	11176±88	-8.6
435	11744±88	-6.6
470	13109±90	-8.4

Although this tuned age model seems plausible compared to other well-dated records from Tibetan lakes, the potential problems in the wiggle-matching approach can result in completely different interpretations of paleoenvironmental changes without detailed examination. First of all, all paleoclimatic proxy data are subject to uncertainties, either in the measurement of the proxies or their age estimates, or both, and these uncertainties

allow data to be adjusted to fit certain hypotheses. We applied no absolute dates to the $\delta^{18}O$ record from Peiku at all and assume that dramatic climate change such the Younger Dryas must have happened in larger spatial scales, i.e. the event was recorded in two

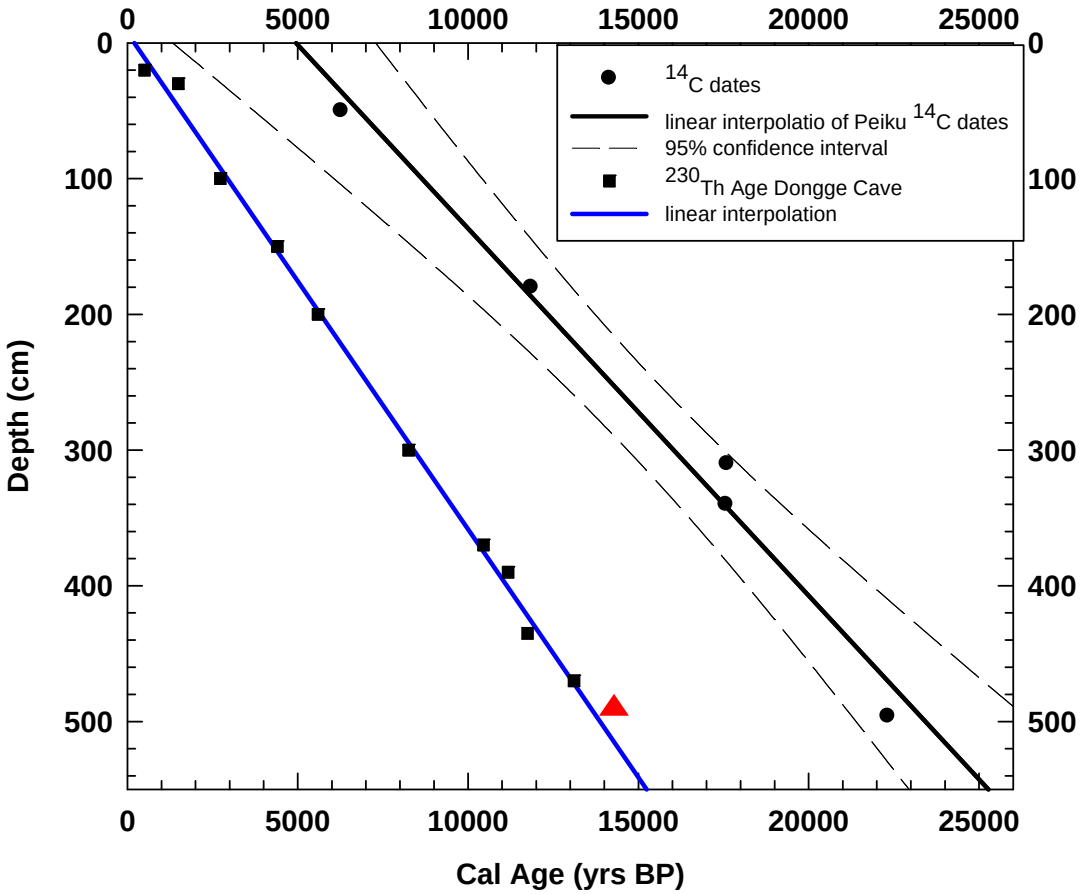

Figure 4.1.3 Age calibration curves from proxy tuning (blue) and ^{14}C dating (black). The new linear interpolation for (blue) estimated ages in Peiku Co is y= 0.0366x-7.5277, R^2=0.9968. The original linear interpolation on ^{14}C dates (black) is y = 0.0262x - 108.15, R^2 = 0.9812. Red triangle denotes the dates of the wood sample.

distant (nearly 2500 km apart) and completely different archives synchronously, though the real timing of the event may be slightly asynchronous even within the Tibetan Plateau (Wang et al., 2002; Morrill, 2004; Huang et al., 2000). For example, the Dongge Cave and Peiku Co are located in totally separate environmental settings, the two ecosystems

are most likely to respond differently to climate variations. Even if two archives seem to be closely correspondent, the underlying mechanisms might be more complex than they appear (Rohling et al., 2009). Second, a degree of subjectivity is involved in deciding which proxy event should be aligned with which proxy peak. In most cases, the chosen age and depth are selected by lining up similar trends, or to a larger extent, by visually comparing the shapes of distinct peaks in different proxy curves. However, more often than not, several peaks that are similar in shape might center at the same age, particularly in high-resolution data sets such as oxygen isotopes, tying such data points together will only result in unreliable age models. On the other hand, low resolution proxy data could make it difficult to identify the exact start and end of certain event, which might cause large chronological uncertainties in climate events as well. The biggest risk associated with wiggle-matching is that once a chronology is set up through tuning climate events between different archives, the resulting chronology loses its chance to assess the timing between these same climate events.

Ideally, more dates should be taken at the same depth of the initial ^{14}C dates on materials less prone to age offsets, e.g. wood or ^{210}Pb. Yet given the limited funding and datable materials, we adopt the tuned chronology as the age-depth reference for this study and further proxy tests are needed to qualify the tuned chronology.

4.2 Total Organic Carbon (TOC) and carbonate content

Total carbon (TC) and total inorganic carbon (TIC) were measured by UIC carbon coulometer, while total organic carbon (TOC) was determined by the difference between

TC and TIC. Assuming most of the TIC in Peiku Co was derived from low-magnesium carbonate, the $CaCO_3$ content can be estimated through multiplying TIC% by 8.33.

TOC values ranges from 0.08% to 2.02% in core PC07-1B, with an average of 0.57%. The lowest TOC value occurred at 15,082 cal BP while the highest value is noted at 12,492 cal BP (Figure 4.2.1). As discussed in the chronology section, the bottom 12 cm is mainly shallow water deposits, thus its age cannot be accurately estimated using the current age model.

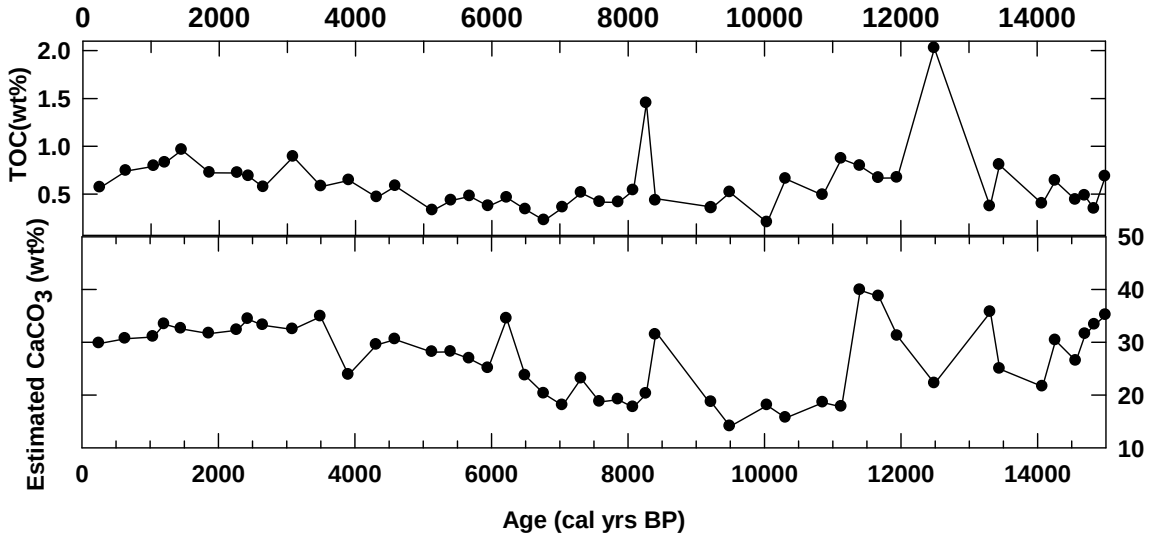

Figure 4.2.1 TOC estimated carbonate content of Peiku Co in weight percentage (wt %)

Likewise, the TOC content in this depth interval is likely not a good indicator of lake Peiku's primary productivity. This paper will focus on the proxy interpretations at depth between 0—538 cm, corresponding to an age range from 0.25 ka BP to 15 ka BP.

The TOC values started to increase after 15 ka BP and appeared to fluctuate between 15 ka BP and 13.3 ka BP. A dramatic increase began in 13.3 ka BP and reached its peak

at ~12.5 ka BP, after which the TOC dropped significantly and remained stable until 11.5 ka BP.

Four proxy events can be seen in TOC records through the Holocene. The first short spell occurred during 10.3—9.5 ka BP, when the TOC dropped to a minimum. The second event took place ~8.2 ka BP, which is marked by a significant decline of TOC content. The third period with lower TOC can be identified between 7.4 ka BP and 6.5 ka BP. The fourth period of slightly elevated TOC value was seen between 5.5 ka BP and 4.5 ka BP. The TOC value increased after 5.0 ka BP and reached another peak around 3.0 ka BP. The TOC value began to decrease during the late Holocene. These short-term changes in TOC content may reflect the changes in precipitation and temperature, yet the low resolution of this proxy makes the identification of these events more difficult.

The estimated calcium carbonate concentration (Figure 4.2.1 lower panel) started to decline after 15 ka BP and reached the first low value at ~14 ka BP. A steady increase in the preservation of carbonates between 14 ka—13.3 ka BP was followed by a dramatic decrease until 12.5 ka BP, the $CaCO_3$ increased afterward and reached a peak around 11.4 ka BP. This trough of decreased carbonate deposition is coincident with the TOC spike. An abrupt drop in carbonate content (from 40 wt % to 17 wt %) occurred after 11.4 ka BP. The carbonate concentrations remained low during the period from 11 ka BP to 9 ka BP, preceding a spike at 8.2 ka BP. The carbonate content continued to increase but was interrupted by a short spell of lower carbonates from 4.5—3.5 ka BP, after which the carbonate concentration gradually declined.

4.3 XRF elemental data

The ITRAX scanner uses X-ray fluorescence to measure the elemental composition of core sediments and can detect the abundance of 26 elements. Some of the elements did not yield reliable results due to low abundance, while other elements may not be of paleoclimatic significance in Peiku Co. Only those elements that are considered to be indicative of paleoenvironmental changes (e.g. Ca, Si, K) are used for discussion here. The results were normalized to the conservative element Ti to minimize variability associated with dilution by carbonates, biogenic silica, or organic matter (Brown et al., 2000).

Eight concurrent peaks (with age of 4780 cal BP, 6250 cal BP, 7350 cal BP, 8900 cal BP, 10,600 cal BP, 10,740 cal BP, 11,520 cal BP and 12,020 cal BP, respectively) occurred in all the XRF curves (Figure 4.3.1), each lasting for a period of no more than 50 years. Judging by the short duration of time and the extremely anomalous values of XRF counts during these events, these transient features are most likely to be caused by episodic tectonic activity such as earthquakes, which appear to have occurred at an interval between 800-1700 years. Further investigation of regional tectonic events would provide more information to help explain these features. These peaks are excluded from the dataset for the purpose of paleoclimate interpretation. All the XRF curves were then smoothed using a negative exponential smoother (SigmaPlot 11.0) by weighting the data in a neighborhood of the smoothing location and applying non-linear methods to combine the weighted values to produce a smoothed value.

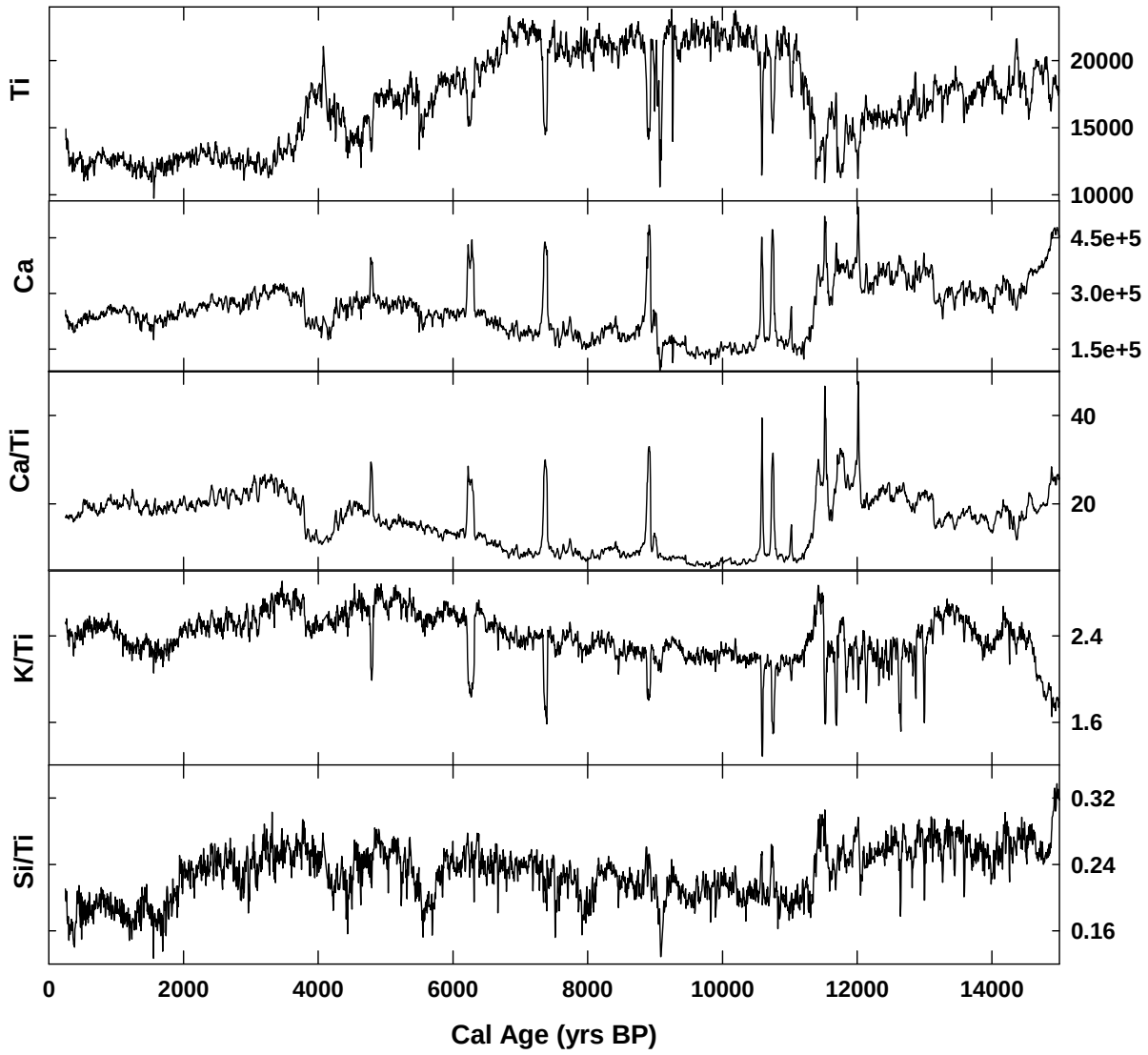

Figure 4.3.1 Raw XRF data. Units of single element are in counts per seconds (cps)

The XRF curves including Ca, K, and Si exhibit a close correlation throughout the whole core. The greatest variability occurred ~11.5 ka BP in all the elemental data. The Ti-normalized Ca value (Ca/Ti) generally follows the non-normalized Ca value, which decreased from 15 ka BP to 13.3 ka BP and began to increase until its peak by 11.5 ka BP. A dramatic decline following ~11.5 ka BP is shown in the Ca, K, and Si curves. The

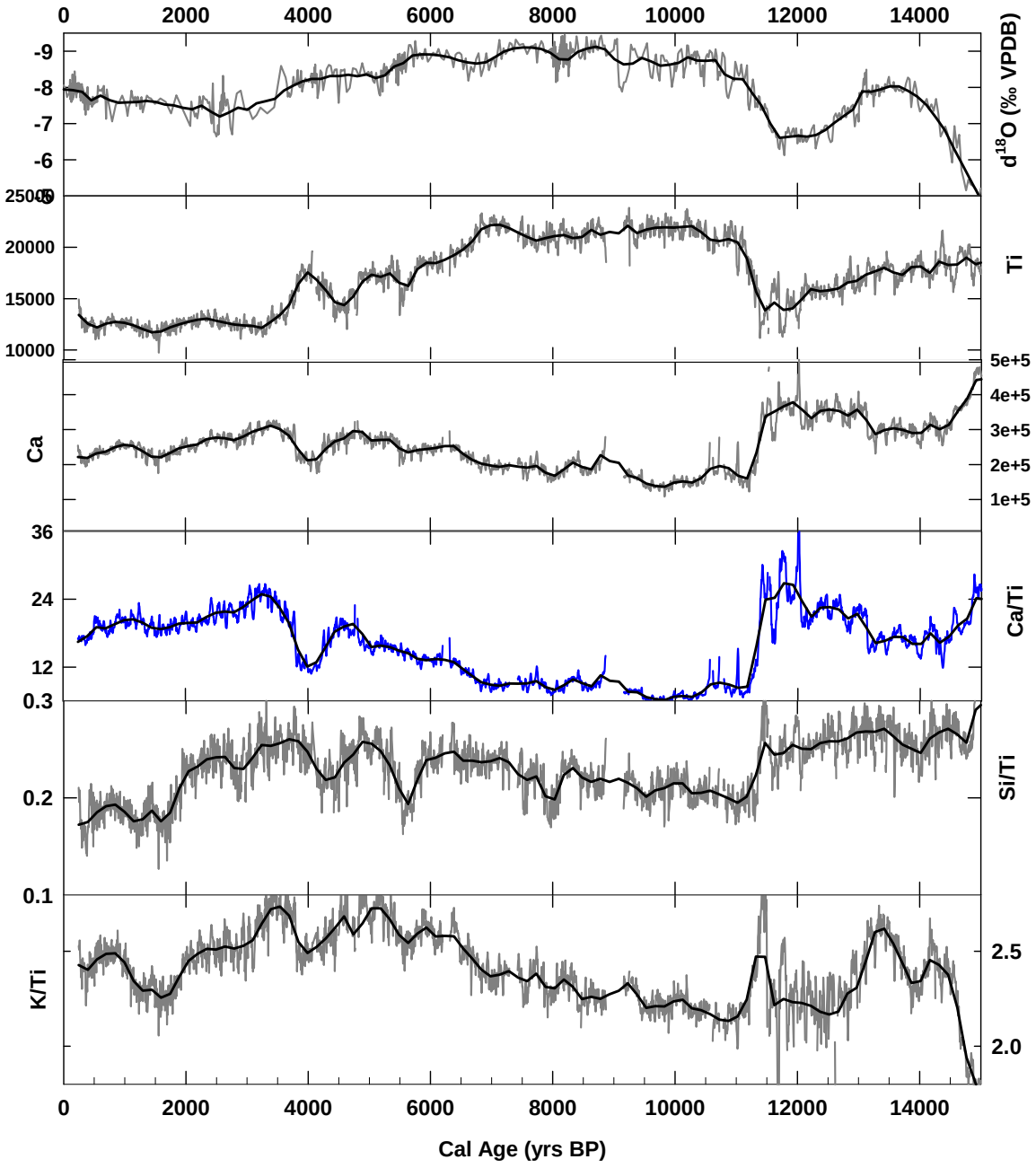

Figure 4.3.2 $\delta^{18}O$ record of stalagmite calcite from Dongge Cave, China (Dykosiki et al, 2005) and XRF elemental data from PC07-1B with presumed tectonic events removed. Single elemental data is given in counts per seconds (cps).

concentration of these elements gradually increased in the next 8000 years before reaching another peak at 3.5 ka BP. A short-term decrease interrupted the overall trend between 3.5—4.5 ka BP. Both the Ca and Ca/Ti started to decline after 3.5 ka BP and similar patterns were indicated in other elements (e.g. K and Si) as well (Figure 4.3.2). Overall, the elemental composition displayed a high consistency through the last 15,000 years.

4.4 Compound-specific carbon isotopes of fatty acids

4.4.1 Fatty acids abundance and distributions

Average fatty acid concentrations in Peiku Co are generally low, ranging from 0 μg/g dry weight to 0.08 μg/g dry weight. The distribution of n-fatty acids through the core shows a strong even-over-odd dominance in chain length from C_{14} to C_{30} (Figure 4.4.1). There are significant concentration differences between individual n-fatty acids.

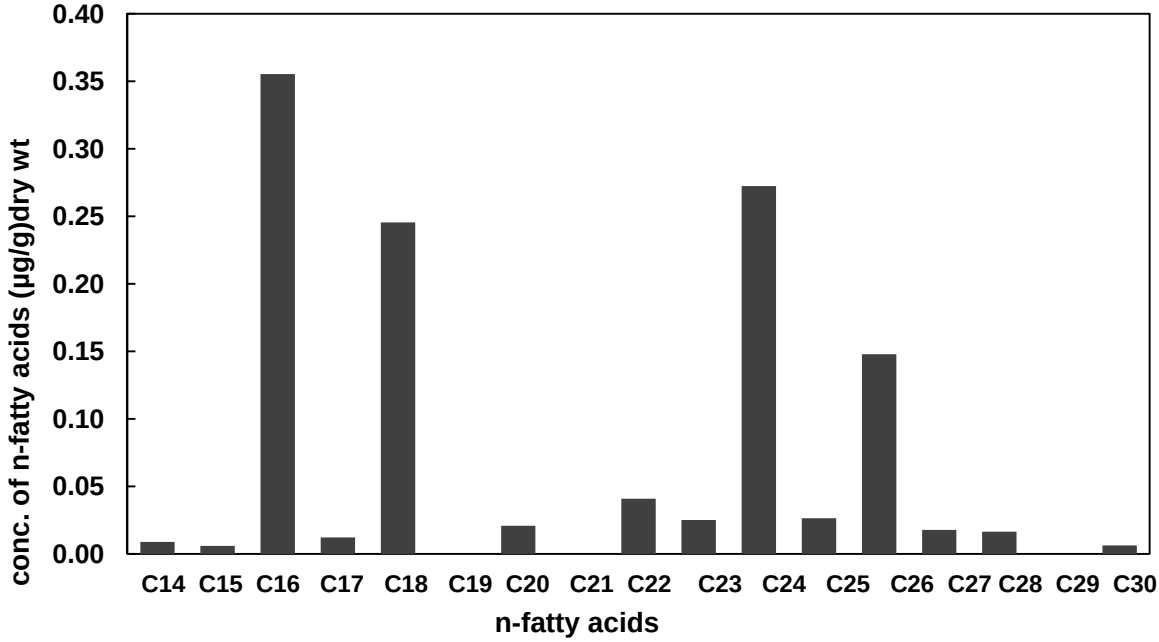

Figure 4.4.1 Mean concentration (μg/g dry weight) and composition of n-fatty acids of core PC07-1B

The short-chain ($<C_{20}$) fatty acids are dominated by C_{16} (palmitic acid) and to a lesser extent C_{18}. The abundances of long-chain ($\geq C_{24}$) fatty acids exhibit higher concentrations at C_{24} and C_{26}. Fatty acids of odd carbon number34 including C_{19}, C_{21} and C_{29} were not detected in the core. The average chain length (ACL) of C_{24}-C_{30} homologs varies between 24.0 and 26.2, with an average value of 24.6 (APPENDIX Table 2).

4.4.2 $\delta^{13}C$ variations of n-fatty acids

The $\delta^{13}C$ results were corrected for the isotopic composition of the methyl group added to the compounds during methylation to ensure that the reported values reflect the $\delta^{13}C$ of the original fatty acids (APPENDIX Table 3). The $\delta^{13}C$ values for C_{28} acid in most samples were not determined by the GC-C-IRMS due to its low abundance. The C_{24} and C_{26} in the bottom three samples were not abundant enough for carbon isotopic analysis. The carbon isotopic values of terrestrial plant fatty acids C_{24} and C_{26} exhibit similar general patterns, ranging from about -24‰ to -30‰ with C_{26} consistently more ^{13}C-depleted (Figure 4.4.2). The $\delta^{13}C$ values of C_{24} fatty acid vary from -22.96‰ to -28.60‰, with an average of -25.85‰. The carbon isotopic values fluctuated yet displayed relatively constant values of -25.09‰ from 14.7 ka BP to that of -26.27‰ noted at 8.4 ka BP. The $\delta^{13}C$ values dropped from -26.35‰ to -28.60‰ during 8.3—7.3 ka BP, preceding the steady increase from 7.3 ka BP until 3.5 ka BP, when the highest $\delta^{13}C$ value of -22.96‰ is noted. The $\delta^{13}C$ values of terrestrial fatty acids moved towards more ^{13}C-depleted values after 3.5 ka BP.

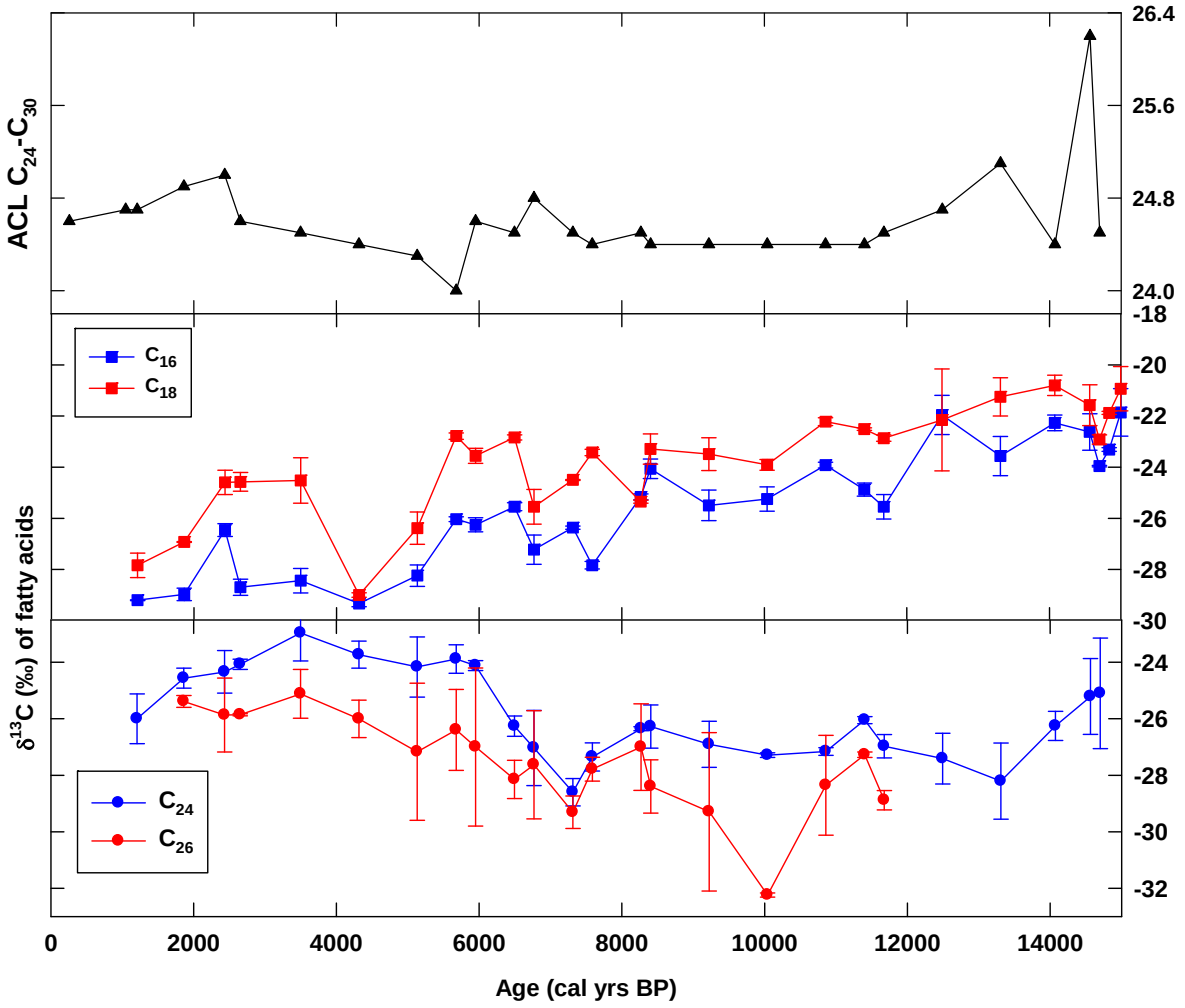

Figure 4.4.2 ACL of fatty acids C_{24}-C_{30} (upper panel), $\delta^{13}C$ measurements of C_{16}, C_{18} (middle panel), and C_{24}, C_{26} fatty acids (lower panel). Error bars representing reproducibility are shown.

The $\delta^{13}C$ of aquatic fatty acids C_{16} and C_{18} parallel each other. The corrected carbon isotopic values of the C_{16} fatty acid (the most abundant of the short-chain n-alkanoic acid) exhibit a relatively large range and vary from -21.86‰ to -29.33‰ (Figure 4.4.2), while those of the C_{18} n-alkanoic acid range from -20.73‰ to -29.00‰. Both aquatic carbon isotopic values show successively decreasing trend from 15 ka BP to 4.3 ka BP, with a plateau to more ^{13}C-enriched values from 6.5 ka BP to 5.7 ka BP. The period between 4.3

ka BP and 3.4 ka BP was marked by increased $\delta^{13}C$ values, followed by a general trend toward ^{13}C-depleted values after 3.5 ka BP.

4.5 GDGT indices

The BIT index of all the 30 samples analyzed showed great variations with high values from 0.23 to 0.88, with the lowest value at core-top, and the highest values at the bottom (Figure 4.5.1). The TEX_{86}-based mean annual lake surface temperature (ALST) varies from 5.6—25.6°C. The overly high temperatures correspond to high BIT values between 0.58 and 0.88, and these high temperature values are considered to be inaccurate due to high terrestrial organic matter input (see discussion section). The MBT-derived MAAT at the core-top is -3.2°C, closely reflecting the measured MAAT (-4°C) on the Tibetan Plateau. The core top sample yields a CBT-derived pH of 8.7, which broadly agrees with the soil pH (6—10) from the Tibetan Plateau, considering the overall error in the range of 1 pH unit (Weijiers et al., 2007). The MAAT and soil pH paralleled with each other. The MAAT decreased from 2.5°C to -6.9°C from 14.6—14 ka BP, followed by an increase to 2.0°C around 12.5 ka BP. The air temperature dropped significantly in the next 2500 years, hitting the lowest point of -7.6°C around 10 ka BP. The temperature showed a warming trend between 9.5—3.4 ka BP, with a steady increase by nearly 10°C. Yet this warming trend was disturbed by a short cooling event characterized by a 3°C drop between 8.4 ka BP and 7.8 ka BP. Another cooling event with the same temperature change occurred between 2.4—1.9 ka BP. The variations in soil pH closely followed the change of air temperature.

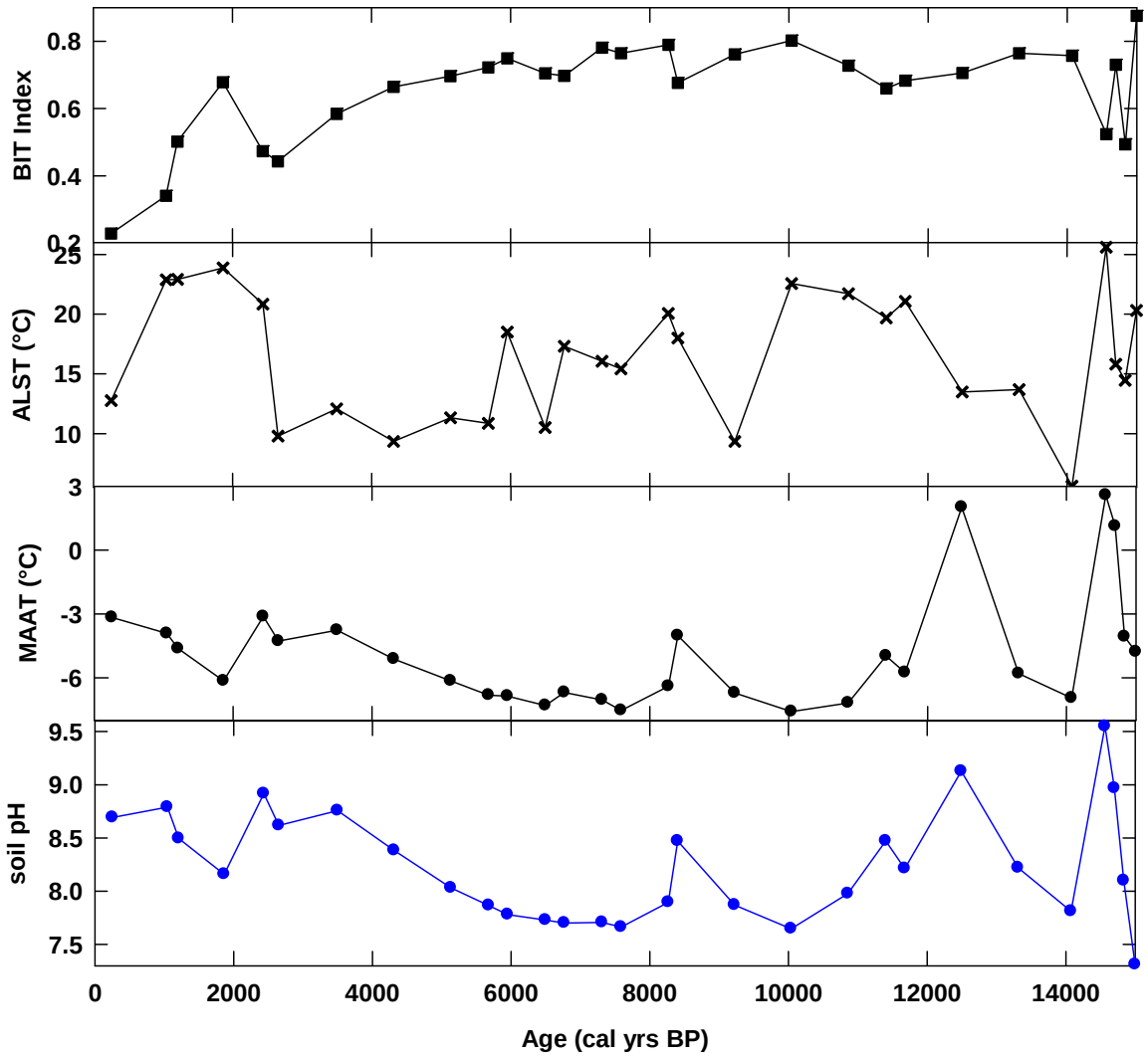

Figure 4.5.1 BIT index, annual mean lake surface temperature (ALST), mean annual air temperature (MAAT) and soil pH (calculations are based on equations in 2.3.2)

5. Discussion

5.1. TOC and carbonate preservation

Total organic carbon (TOC) is often used as a fundamental proxy of true primary productivity in lacustrine sediments. Yet it could come from multiple sources (aquatic,

bacterial and terrestrial), and it may also be affected by the degree of remineralization. In addition, the organic carbon content could be diluted by the addition of clastic sediment particles and concentrated by the dissolution of carbonate minerals in sediment. Therefore, in lacustrine systems, variations in TOC may reflect changes in lake productivity, which is mainly controlled by air temperature fluctuations and nutrient influx, although changing conditions of organic matter preservation could have altered the productivity-TOC relationship (Zhu et al., 2009b), e.g. a decrease in TOC may indicate decreased productivity, decreased organic matter preservation or increased dilution.

The inorganic carbon concentrations may be interpreted as the preservation of carbonate in lake sediments. The mineral composition from X-ray diffraction reveals that the carbonates of Peiku are mostly low-Mg calcite and aragonite, with little high-Mg calcite (A.G. Henderson, personal communication). The solubility of calcium carbonate in natural water is mainly controlled by the simple equilibrium that involves Ca^{2+}, HCO_3^-, CO_3^{2-} and water. Surface water and groundwater is usually saturated with calcium carbonate, and the carbonate may precipitate through the addition of cation (Ca^{2+}) or anion (HCO_3^-) from surface or ground water flows. Moreover, the precipitation of calcium carbonate can be controlled by other factors including temperature, CO_2 concentration, and pH. The solubility of calcium carbonate increases with decreases in temperature; plants may remove CO_2 from the water through photosynthesis, leading to an increase in the pH of the lake water and oversaturation with respect to calcite, which in most cases will cause calcium carbonate to precipitate. This precipitation process prevails under humid climate conditions, while precipitation caused by salinity increases

due to evaporation dominates in arid climates. Counts of calcium (Ca) using an XRF can be used as a proxy for carbonate preservation in the sediment (Figure 5.1.1).

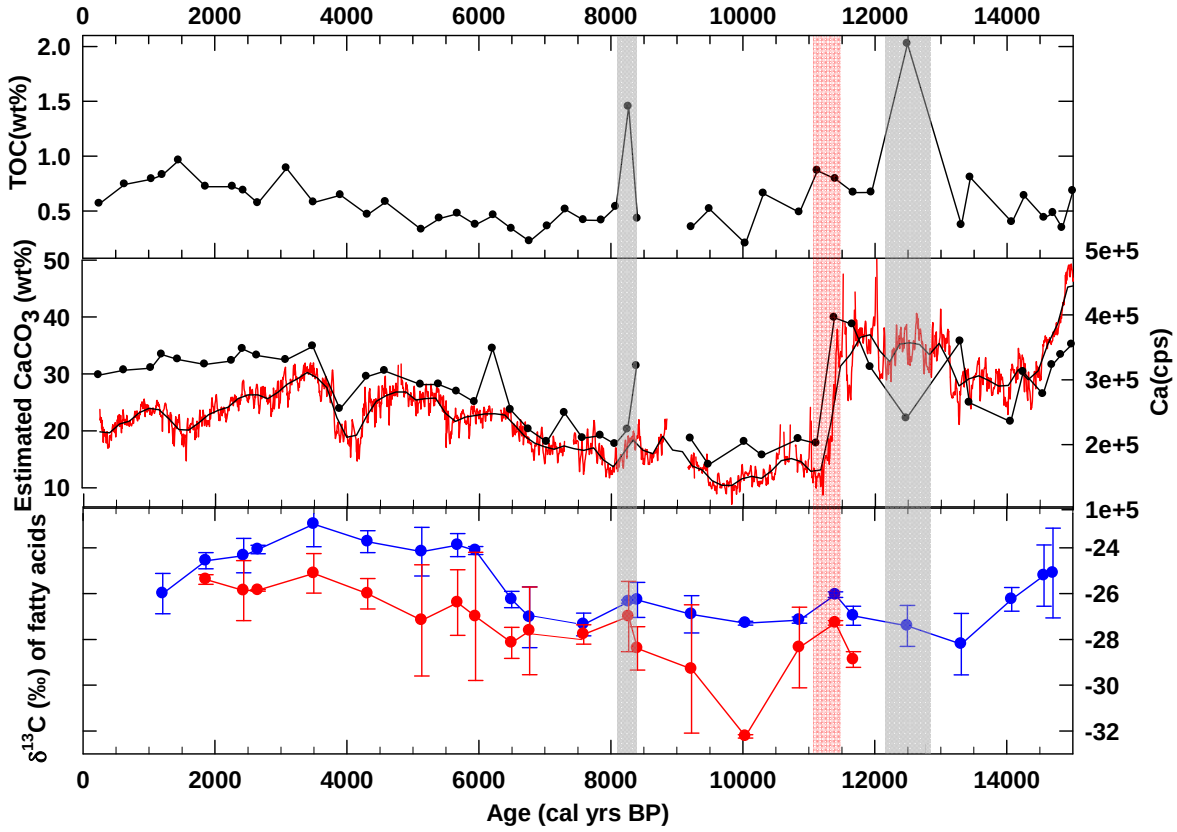

Figure 5.1.1 TOC (upper panel), estimated $CaCO_3$ content (middle panel, dash-dotted line), Ca counts (middle panel, red line), and $\delta^{13}C$ of terrestrial biomarkers C_{24} (blue) and C_{26} (red) of Peiku sediment (lower panel)

The TOC content is generally low during the past 15,000 years, with two exceptions that occurred at 12.5 ka BP and 8.2 ka BP (denoted by gray bars in Figure 5.1.1), respectively. The TOC spikes at 12.5 ka BP would be most likely a piece of wood or leaf trapped in the sediments, as the high TOC value does not correlate to any other proxies in the record. It is also possible that the sediment at this depth is derived from melt water of the glaciers from high altitude, which would carry material of various sources. There are

no corresponding peaks in other proxies that can help explain the peaks at 8.2 ka BP. The increase TOC value from 15 ka BP to 13.3 ka BP probably resulting from enhanced lake productivity or higher nutrient flux due to increased monsoon-induced precipitation during this period. However, the TOC inferred precipitation changes are subject to large uncertainties due to the low values and low resolution.

The estimated $CaCO_3$ content is highly consistent with Ca counts. High $CaCO_3$ content throughout the record suggests lake water is saturated with calcium carbonate, and the precipitation of carbonates is a result of increased salinity due to stronger evaporation and less riverine input under arid conditions. The increase in carbonate preservation between 13.3—11.5 ka BP indicate drier climate during this period. The lake may have become hydrologically open due to increased precipitation or a dramatic discharge of glacier meltwater from the surrounding mountains, causing a sudden drop in calcium concentration (marked by the red bar) after 11.5 ka BP, until the lake surface regained its original level. This event is also evident in other elemental proxies of Peiku Co (see Section 5.2). The Ca concentration remained low during the early-Holocene, suggesting the lake basin was open while humid conditions prevailed during this period. The carbonate content gradually increased, which may correspond to a return to closed basin conditions and a more arid climate, from 7.0 ka BP to 3.5 ka BP when enhanced evaporation caused the lake water to be more saline. The declining trend after 3.5 ka BP suggests a return to wetter conditions.

5.2 Elemental proxy interpretation

Rb/Sr ratio has been used as a proxy for monsoon intensity (An et al., 2011). Rubidium (Rb) is incorporated mainly in potassium (K)–bearing silicates and exhibits inert geochemical behavior, while strontium (Sr) can substitute for calcium (Ca) in the lattices of carbonates. Previous studies have shown that the Rb/Sr ratio in weathering residue increases as weathering intensity increases due to a higher Sr activity and a more inert nature of Rb (Chen et al., 1999). A study on Cuoe Lake (central Tibet) suggests that the more inert Rb was carried into the basin together with the silicate input resulting from physical weathering, whereas the Sr was leached into solution during chemical weathering and was transported as dissolved Sr^{2+} (Wu et al., 2006). Accordingly, stronger chemical weathering leads to more dissolved Sr^{2+} being transported into the depositional basin. If the lake basin is closed, more Sr^{2+} will precipitate with that of the carbonates, while the ratio can be complicated when the lake basin is open, since Sr^{2+} leaves the system in the outflowing rivers.

K can be indicative of the weathered clastic sediment, as it is preferentially removed in chemical weathering. Higher K/Ti ratios in the lake sediment could be indicative of more input of unaltered fresh source materials (Nath et al., 2000). Changes in the transport efficiency of weathered materials can result from variations in precipitation. As precipitation increases, enhanced stream power can erode and transport chemically altered material that accumulated on land during period of dry climate. Therefore, it is assumed that the concentration of clastic materials in the sediment, including K, Fe, Si, mainly reflect changes in fluvial transportation from the catchment.

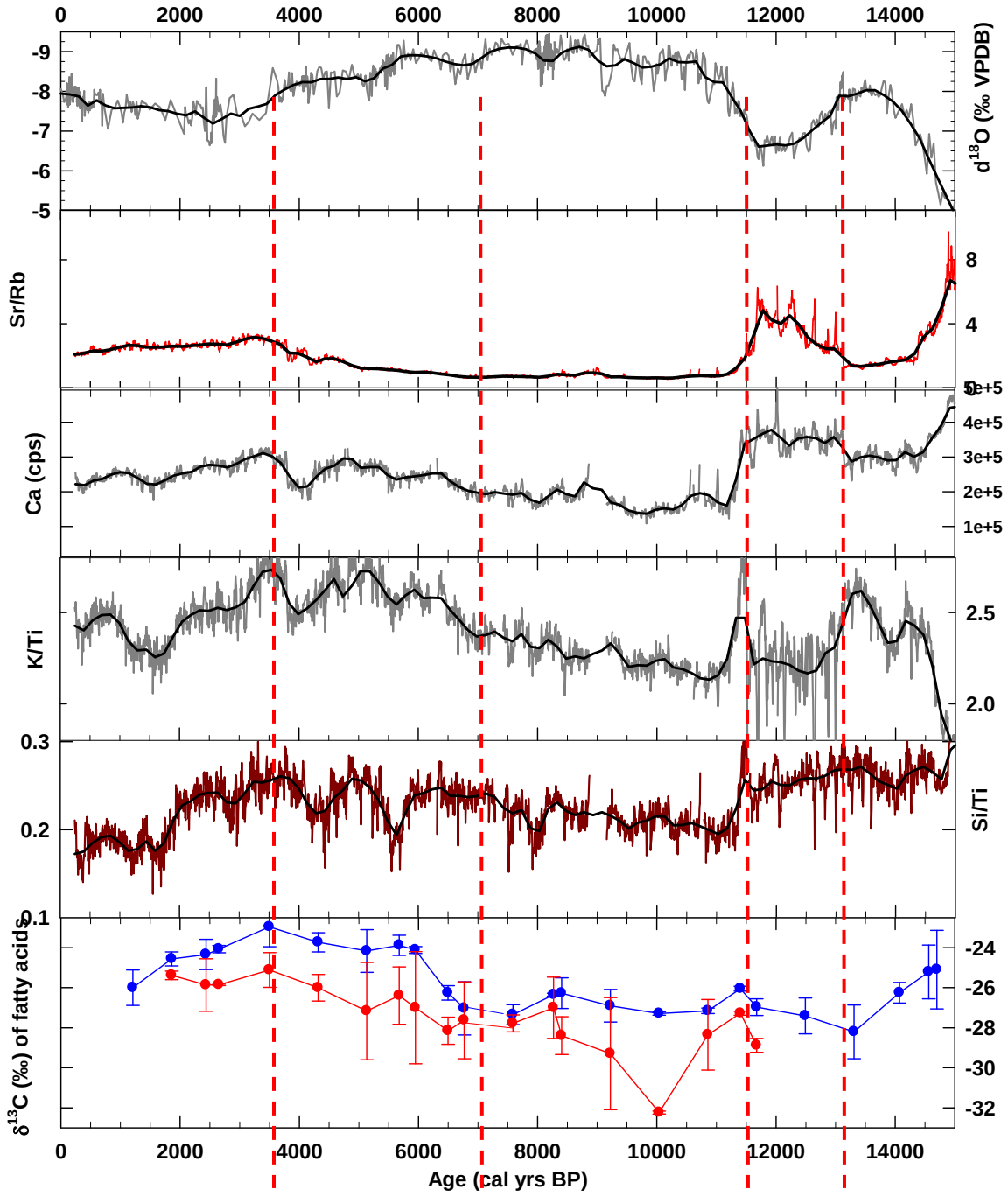

Figure 5.2.1 $\delta^{18}O$ of Dongge Cave (Dykoski et al, 2005), Sr/Rb ratio, Ca counts and normalized-K, Si data from Peiku Co, and $\delta^{13}C$ data of terrestrial biomarkers C_{24} (blue) and C_{26} (red)

The elemental data for Ca, K/Ti, Si/Ti show the same patterns over most of the record. The period between 15 ka BP and 13.3 ka BP featured the transition from an arid period

to a more humid interval. The decreased Ca may be a result of increased precipitation and less evaporation in the lake. Enhanced precipitation and stream power could facilitate the transport of unaltered material from fresher rocks into the lake, leading to an increased K/Ti value. The wetter conditions would also enhance fluxes of dissolved silica into the lake through increased surface flow. The end of this humid interval was truncated by abrupt changes in all proxies. The increased preservation of carbonate between 13.3—11.5 ka BP could be a response to enhanced evaporation under drier conditions. The abrupt decrease in precipitation can be further confirmed by increased $\delta^{18}O$ of ostracodes from the same core (Figure 4.1.2). Increases in K/Ti and Si/Ti ratios towards the end of this dry interval suggest a return to wetter climate. The dramatic decreases in all proxies indicate rapidly developed humid climate after 11.5 ka BP, as also reflected by the $\delta^{18}O$ record. As discussed in the previous section, Peiku Co may have become hydrologically open due to increased precipitation or a dramatic discharge of glacier melt water from the surrounding mountains. The terraces in the northeast and southwest of Peiku Co indicate that lake level was much higher in the past, and the chronology of previously work done on the terraces (Peng, 1997; Huang, 2000) roughly agrees with our interpretation (Figure 5.2.2). Humid conditions prevailed from 11.5 ka BP to 6.7 ka BP, causing lake level rise and enhanced shoreline erosion, which brought more fresh material into the lake basin. Following the humid period, drier conditions developed over the next 1200 years.

5.3 $\delta^{13}C$ of n-alkanoic acids and implications for climatic conditions

Carboxylic acids in lake sediments typically originate from multiple sources. Some are ubiquitous components and major constituents of the lipids of fresh-water algae (i.e. n-C_{16} and n- C_{18} alkanoic acids; Cranwell, 1976), while others derive from leaf wax

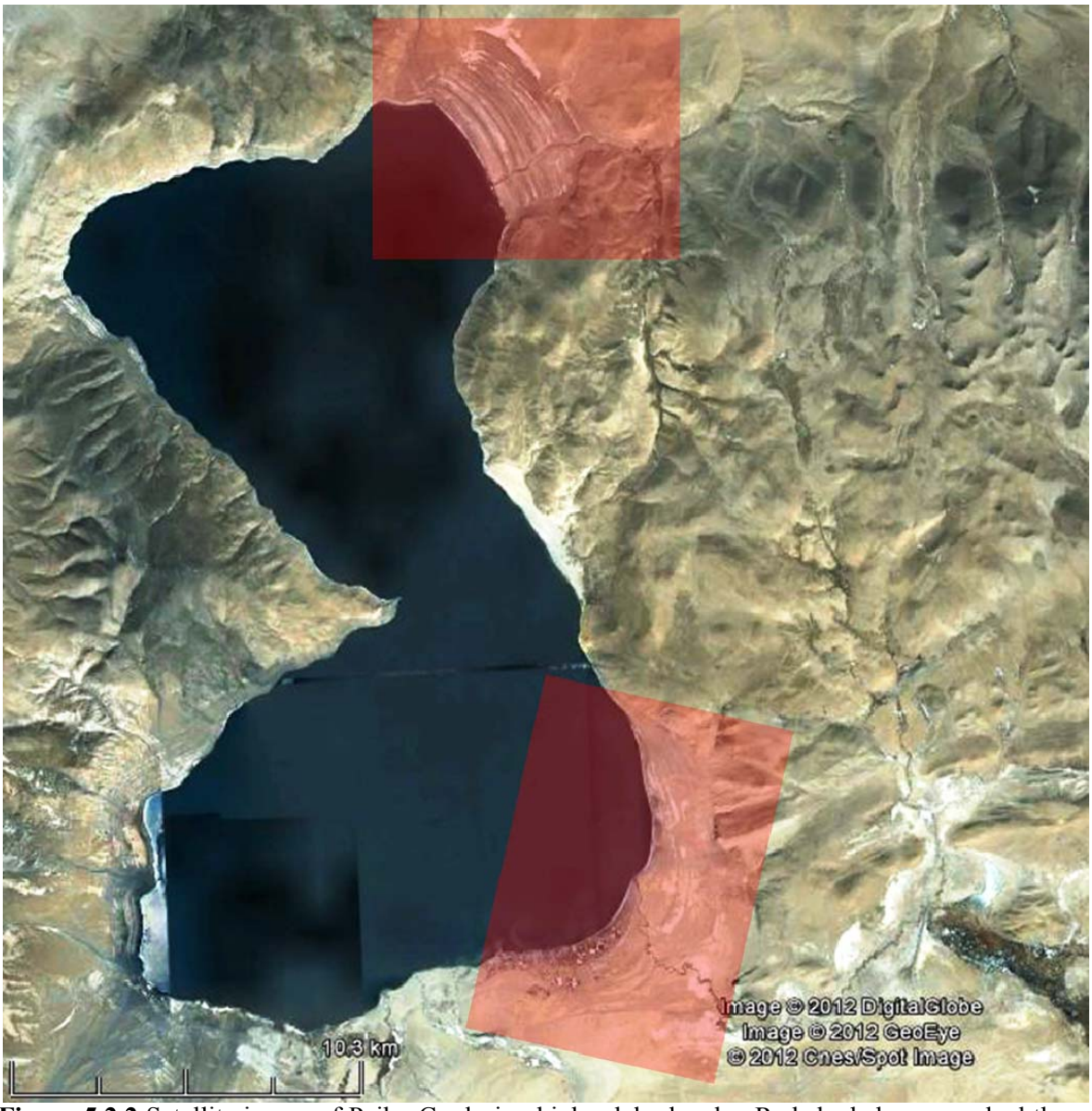

Figure 5.2.2 Satellite image of Peiku Co during higher lake-levels. Red shaded area marked the terraces at the northeast and southeast of the lake that were formed during the fluctuations of lake levels.

coatings of terrestrial plants (the even-chain C_{24}-C_{30} alkanoic acids, Eglinton and Hamilton, 1967). The n-alkanoic acids abundance and distribution in Peiku sediments are characterized by two peaks; C_{16} and C_{24}, indicating significant contributions of terrestrial plants as well as from algae (Figure 4.4.1).

The preservation of terrestrial n-alkanoic acids (C_{24}-C_{30}) in Peiku Co is sufficient to study the vegetation change and provide direct comparisons to other climate proxies from the same core. These compounds have been shown to be transported long distances via aeolian processes, however, studies of lake and marine sediments indicate that the predominant source of plant leaf waxes is generally local vegetation in the surrounding watershed (Hughen et al., 2004). Thus, in a small-sized lake such as Peiku Co, the greatest concentration of plant waxes is mostly likely derived from local sources instead of long-distance transport. The distributional variations in plant biomarkers record differences between the arid and humid vegetation sources. For example, a study on southern Asian paleosols and Bengal Fan sediments show strong correlations between chain-length variability and n-alkane $\delta^{13}C$, reflecting the Miocene expansion of C_4 grasses (Freeman and Colarusso, 2001).

As discussed in the previous sections, C_3 and C_4 plants are adapted to specific conditions. Two types of parameters control the predominance of one photosynthetic pathway over the other: (1) atmospheric CO_2 concentration and (2) climatic parameters, mainly plant available moisture and daytime growing-season temperature (Long, 1999; Sage et al., 1999). At low atmospheric pCO_2, C_4 plants, which use a CO_2-concentrating mechanism, will eventually outcompete C_3 plants. Moreover, C_4 plants cope better with water stress (i.e., low moisture) and high temperatures than C_3 plants. The relative influence of pCO_2 and climate parameters on C_3 and C_4 vegetation is still under heated debate. Recent studies show that pCO_2 evolution alone cannot explain the significant C_3/C_4 changes either for long time scales or for glacial/interglacial transitions. For example, a Miocene pCO_2 reconstruction (Pagani et al., 2005) does not support the

hypothesis that the late Miocene C_4 plant expansion was primarily caused by a pCO_2 decrease. In China and central Africa, greater proportions of C_3 vegetation have been reported during glacial periods characterized by low pCO_2, than for interglacial periods characterized by higher pCO_2 (Huang et al., 2001; Schefuss et al., 2003; An et al., 2005). The $\delta^{13}C$ record from the Himalaya basin (Galy et al, 2008) indicates that C_4 plants declined in the Himalayan basin when both humidity and pCO_2 increased while no significant vegetation change occurred when pCO_2 and humidity changes in opposite directions. Therefore, the LGM to pre-industrial pCO_2 increase cannot fully explain the C_4 plants proportion decrease observed in the Himalayan basin during this period. These studies clearly suggest that regional climate parameters control the relative C_3 and C_4 abundances on land and highlight the predominant influence of humidity.

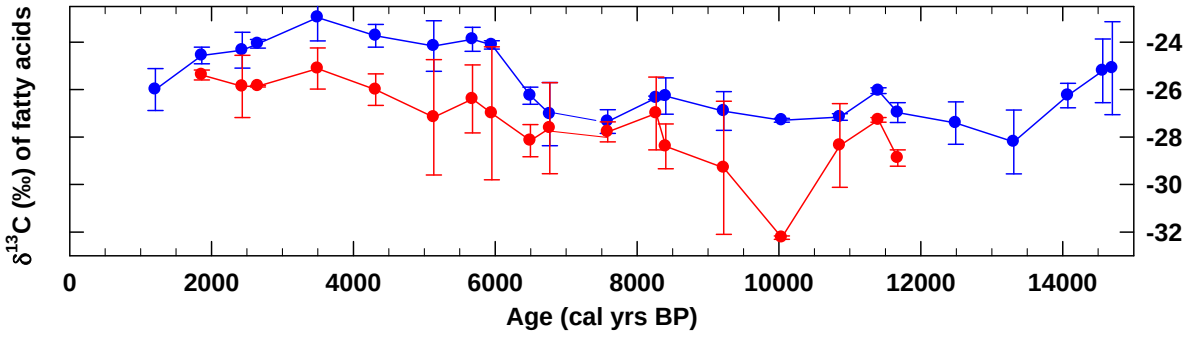

Figure 5.3.1 $\delta^{13}C$ values of long-chain fatty acids C_{24} (blue) and C_{26} (red). Error bars representing reproducibility are shown.

The $\delta^{13}C$ values of long-chain fatty acids were ^{13}C-depleted by 3‰ during the period between 15 ka BP and 13.3 ka BP compared to the value at the beginning of this period (Figure 5.3.1), reflecting a greater portion of waxes from C_3 plants in more humid climates. The $\delta^{13}C$ values were enriched by 2.5‰ between 13.3 ka BP to 11.5 ka BP,

which suggests an increase in C_4 vegetation as climate conditions transition to a more arid period.

The period between 11.5 ka BP and 6.7 ka BP appeared to be relatively humid with little variations in the $\delta^{13}C$ values compared to the interval that followed. The climate evolved towards drier conditions from 6.7 ka BP to 3.5 ka BP, as $\delta^{13}C$ values became more positive until they reached their most enriched value around 3.5 ka BP, with a total enrichment of 4‰, suggesting an extended development of an arid climate, which preceded wetter conditions after 3.5 ka BP.

5.4 Application of the GDGT indices

5.4.1 Validation of TEX_{86}

As the key biomarker for Thaumarchaeota, crenarchaeol was found in the sediments of all 47 surveyed European lakes (Blaga et al., 2009), though in most of the surveyed lakes it was present in relatively minor amounts. In contrast, Powers et al. (2010) found crenarchaeol below detection limits in 24 of the 46 globally distributed lakes that they surveyed.

Nevertheless, the results from Peiku Co show that aquatic Thaumarchaota were present in 29 out of 30 lake sediment samples, with highly variable relative abundances ranging from 12.16% to 65.66% (APPENDIX Table 4). The depth distribution of aquatic Thaumarchaota is found to be variable within marine and lacustrine water columns and a recent study shows that Thaumarchaota are predominantly productive in the upper part of the water column in lacustrine systems, which are exported to the sediments (Sinninghe

Damsté et al., 2009). Yet the physical and chemical character of the lake may affect the diversity and distribution of Archaea in the sediments.

The BIT index values in soils typically range from 0.8 to 1.0, indicating that a significant proportion of thaumarchaeal lipids could derive from soils (Weijers et al., 2006b). In our study, lake sediment BIT index values vary from 0.23 to 0.88, indicating a wide range of soil organic matter inputs (APPENDIX Table 4). The BIT index values of 28 Peiku samples are well above 0.5, suggesting substantial amounts of branched compared to isoprenoid GDGTs, which was reflected by higher relative abundance of soil derived GDGTs. Thus, the TEX_{86} signal was compromised due to the input of soil-derived GDGTs.

5.4.2 Application of MBT/CBT in MAAT and soil pH reconstructions

The MBT/CBT calibration has been successfully applied to reconstruct air temperatures using loess deposits (Peterse et al., 2011), peats (Ballantyne et al., 2010), marine sediments from the Congo Fan (Weijers et al., 2007a), and lacustrine sediments from New Mexico (Fawcett et al., 2011). However, as previously discussed (Section 2.3.2), several problems need to be addressed before branched GDGTs can be successfully applied broadly to lacustrine sediments. It is still unclear if these compounds are derived from eroded soils or if they are produced in situ. Recent studies suggest that MBT/CBT reconstructed MAAT are much lower than the observed MAAT using the soil based calibrations (Weijers et al., 2007b) in tropical (Tierney et al., 2010) and temperate (Blaga et al., 2010) regions. Moreover, the study on soils in East Africa indicates that MBT/CBT reconstructed temperatures decreased with increasing altitude, but

reconstructed temperatures differed from the measured air temperatures, suggesting that local calibrations are needed to constrain the MAAT reconstructions (Sinninghe Damsté et al., 2008). To better understand environmental controls on the distributions and the sources of branched GDGTs in lake sediments, Loomis et al. (2011) compared the branched GDGT distributions and concentrations in lake sediments and catchment soils within a 3600 m altitudinal gradient in western Uganda. The results suggest that there are significant offsets between observed and reconstructed MAAT from wet, high elevation soils but not in most dry, low elevation soils, which provide further evidence that branched GDGTs might be produced in situ in lakes Therefore, this temperature proxy in lacustrine systems with high soil loadings should be used with caution. In contrast, reconstructed pH values are much closer to measured values at all elevations (Loomis et al., 2011).

The reconstructed MAAT of core-top sediment in Peiku Co is -3.2°C, closely reflecting the measured MAAT (-4°C) on the Tibetan Plateau. The CBT-derived pH of core-top sediment is 8.7, which roughly agrees with the soil pH (6—10) from the Tibetan Plateau, given the error of 1 pH unit (Weijiers et al., 2007). Yet strong correlation between reconstructed MAAT and pH suggests that the reconstructions are not robust. In additions, lack of long-term instrumental temperature record in this area make it difficult to validate its reliability. Therefore, these two paleothermometers are not used for paleoclimate reconstructions in the end. Further calibration needs to be developed to produce reliable temperature records for the Tibetan Plateau.

5.5 Paleoenvironmental history of the past 15,000 years in Peiku Co

The trends in the biomarker data and other geochemical proxies are complex and interpretation of the paleoenvironmental history of Peiku Co over the past 15 ka does not always provide straightforward answers. For this reason, the record was divided into major climate intervals based on the overall trends, but the variations in the individual climate proxies do not always align with these intervals (Figure 5.5.1).

Stage 1 (15 ka—13.3 ka BP): This interval is characterized by increasing K/Ti values, relatively constant yet high Si/Ti values and declined Ca values, suggesting a transition from a dry period to humid conditions. During the interglacial, lake productivity increased as temperature and monsoon-induced precipitation favored photosynthesis and provided a rich nutrient supply. It is possible that elevated K/Ti and high Si/Ti levels were caused by higher runoff due to enhanced precipitation. The $\delta^{13}C$ values of terrestrial biomarkers were depleted by 3‰ during the period between 15 ka BP and 13.3 ka BP, indicating greater portions of C_3 vegetation in this area, which also confirms that climate moved toward more humid conditions.

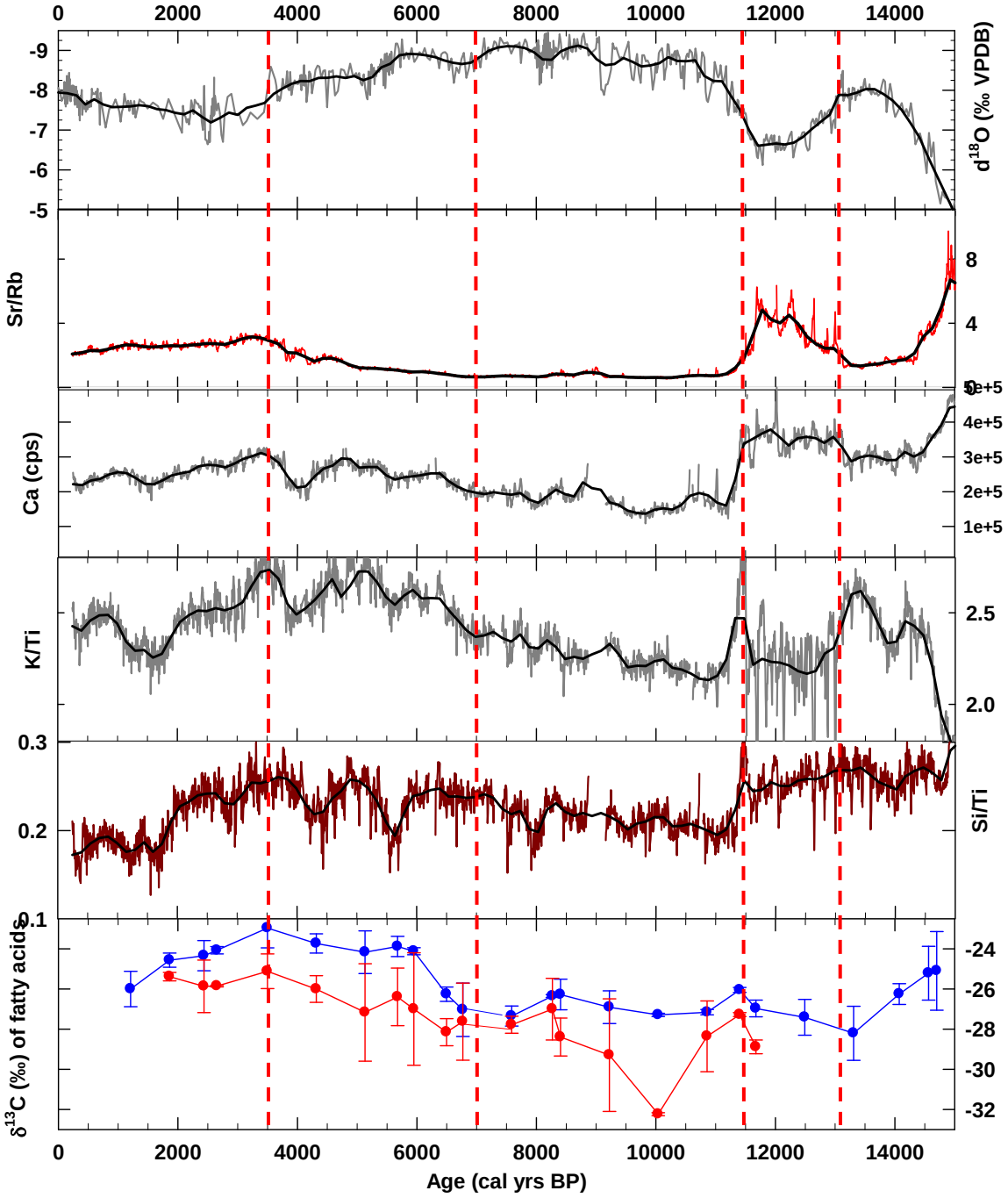

Figure 5.5.1 Proxies used for paleoclimatic interpretation in this study. The $\delta^{18}O$ data is from Dongge Cave (Dykoski et al. (2005).

Stage 2 (13.3 ka—11.5 ka BP): This period featured ^{18}O-enrichment in the ostracod record (Figure 4.1.2) and ^{13}C-enrichment in terrestrial plant leaf waxes, suggesting drier conditions dominated this area and C_4 vegetation expanded during this ~1800 ka interval.

Stage 3 (11.5 ka—6.7 ka BP): The increased Ca/Ti, K/Ti and Si/Ti ratios towards the end of Stage 2 marked the onset of a wetter climate. The dramatic decreases in all proxies at the start of Stage 3 indicate a humid interval after 11.5 ka BP, as is also reflected by a depletion of 6.5‰ in the $\delta^{18}O$ record (Figure 4.1.2). The humid conditions remained stable from 11.5 ka BP to 6.7 ka BP, causing lake level rise and enhanced shoreline erosion, which brought more chemically altered material into the lake basin. The $\delta^{13}C$ value slightly dropped, suggesting expanded development of C_3 vegetation.

Stage 4 (6.7 ka—3.5 ka BP): The Ca/Ti progressively increased, which may result from a dry climate. The fluctuations in K/Ti and Si/Ti could be caused by more wind-driven transport of clastic material into the lake. The Fe/Ti remained low as a result of decreased surface or groundwater inflow. C_4 plants continued to expand after 6.7 ka BP, displayed by a 4‰ enrichment of ^{13}C in terrestrial biomarkers.

Stage 5 (after 3.5 ka BP): The more negative $\delta^{13}C$ values suggest climate evolved towards more humid conditions after 3.5 ka BP. Increased precipitation could cause lake level rises, bringing more altered material into the lake basin via enhanced stream power, as reflected from lowered K/Ti and Si/Ti.

5.6 Comparisons with other records from the Tibetan Plateau

A multi-proxy study on Lake Ximencuo (eastern Tibetan Plateau) identified six cold events during the Holocene, which occurred between 10.3–10.0 ka BP, 7.9–7.4 ka BP,

5.9–5.5 ka BP, 4.2–2.8 ka BP, 1.7–1.3 ka BP and 0.6–0.1 ka BP (Mischke et al., 2010) Comparisons with previously published Holocene records from lake sediments, ice cores and glacial remains of the Tibetan Plateau (Gasse et al., 1996; Thompson et al., 1997; Zhu et al., 2009b; Wu et al., 2006; Morrill et al., 2006; Yao and Thompson, 1992; Shen et al., 2005) revealed that the cold event that occurred at 4.2 ka BP registered in almost all previous studies. However, this cold event could not be found in the geochemical record in Peiku Co (southern Tibetan Plateau), likely because of 1) low resolution of climate proxies, 2) age differences cause by wiggle-matching, or 3) certain catchment-specific events that compromised the true climate signals.

The cold event inferred between 7.9 and 7.4 ka BP from Lake Ximencuo was recorded at a number of sites on the eastern Tibetan Plateau (Shen et al., 2005) and probably corresponds to a cold event identified around 8.2 cal ka BP at the sites on the western central Tibetan Plateau (Gasse et al., 1996). The short-term cooling could be identified from the $\delta^{18}O$ record and to a lesser extent, the $\delta^{13}C$ value terrestrial plants in Peiku, while this cool episode was missing in other proxies from this lake. It is possible that local events such as turbidity currents and slumping muted the weak signal. Nevertheless, the strong correlation in $\delta^{18}O$ of Peiku Co with the 8.2 ka event of the North Atlantic region support that that latter had a expanded influence on southern Tibet as well.

Previous investigations suggest that the Holocene Climatic Optimum on the Tibetan Plateau occurred during the early to mid Holocene as a result of the early Holocene insolation maximum in low latitudes of the northern hemisphere and an increase in monsoon strength (Lister et al., 1991; Van Campo and Gasse, 1993; Berger and Loutre,

1991). Nevertheless, recent studies indicate a more complex pattern of Holocene climate change and diachronous environmental response on the Tibetan Plateau (An et al., 2000; Herzschuh, 2006). This complex pattern may be caused by the interplay of major atmospheric circulation systems, which serve as the moisture sources of this region as well as the balance between precipitation and evaporation in different areas of the Tibetan Plateau. Most studies assume that warmer conditions are always associated with wetter climate, yet stronger summer monsoons with increased cloudiness may also result in cooler and wetter conditions.

6. CONCLUSIONS

The multi-proxy record of Peiku Co, including oxygen isotopes of ostracodes, elemental composition, and carbon isotopes of biomarkers, provides a paleoenvironmental history of the adjacent region on the southern Tibetan Plateau. The chronology is constrained by ten tie-points between high-resolution Peiku oxygen isotope records from ostracod assemblages and independently dated record from Dongge Cave. This study shows that the lake sediments contain multiple climate-sensitive proxies that are related to the dominance of major atmospheric circulation systems that influence the region. The climate of Peiku basin transitioned to wetter conditions after 15 ka BP, followed by an arid event between 13 ka and 11.5 ka BP, likely correlating to the Younger Dryas. The early- to mid-Holocene climate was characterized by wetter conditions, while drier climate prevailed after 6.7 ka BP. The climate of late-Holocene returned to wetter conditions, probably due to stronger SW monsoons.

The cold event at 8.2 ka BP and widespread event at 4.2 ka BP could not be distinctively identified in all the proxy records from Peiku Co. The timing of Holocene events are further complicated by the wiggle-matching approach employed.

The application of the BIT index indicated a constantly high amount of soil organic matter input to the lake, which biased the mean annual lake surface temperature as reconstructed by TEX_{86}. Most Tibetan lakes are greatly influenced by the riverine supply, resulting in high BIT values. Further study of the GDGT distribution in soil, water column and lake sediments are needed for a better regional calibration of lake surface temperature and air temperature.

7. REFERENCES

An, Z. S. et al. (2000) The history and variability of the East Asian palaeomonsoon climate. Quaternary Science Reviews 19, 171–187.

An, Z., Kutzbach, J.E., Warren, L.P., Porter, S.C., (2001). Evolution of Asian monsoon and phased uplift of Himalaya–Tibetan Plateau since late Miocene times. Nature 411, 62–66.

An, Z. S., S. C. Clemens, et al. (2011). Glacial-Interglacial Indian Summer Monsoon Dynamics. Science 333(6043): 719-723.

Bard,E. Comparison of alkenone estimates with otherpalaeotemperature proxies, Geochem. Geophys. Geosyst. 2 (2001) 2000GC000050.

Bechtel, A., R. H. Smittenberg, et al. (2010). Distribution of branched and isoprenoid tetraether lipids in an oligotrophic and a eutrophic Swiss lake: Insights into sources and GDGT-based proxies. Organic Geochemistry 41(8): 822-832.

Berger, A. and Loutre, M.F. 1991. Insolation values for the climate of the last 10 million years. Quaternary Science Reviews 10: 297-317

Blaauw, M. (2010). Methods and code for 'classical' age-modelling of radiocarbon sequences. Quaternary Geochronology 5(5): 512-518.

Blaga, C.I., Reichart, G.–J., Heiri, O., Sinninghe Damsté, J.S., 2009. Tetraether membrane lipid distributions in water-column particulate matter and sediments: a study of 47 European lakes along a north–south transect. Journal of Paleolimnology 41, 523–540.

S.C Brassell, R.G Brereton, G Eglinton, J Grimalt, G Liebezeit, I.T Marlowe, U Pflaumann and M Sarnthein, Palaeoclimatic signals recognized by chemometric treatment of molecular stratigraphic data. Org. Geochem., 10 (1986), pp. 661–669.

Brown, E. T., R. Bendick, et al. (2003). Early Holocene climate recorded in geomorphological features in Western Tibet. Palaeogeography, Palaeoclimatology, Palaeoecology 199(1–2): 141-151.

Brown, E. T. (2011). Lake Malawi's response to "megadrought" terminations: Sedimentary records of flooding, weathering and erosion. Palaeogeography, Palaeoclimatology, Palaeoecology 303(1-4): 120-125.

Burnett, A. P., M. J. Soreghan, et al. (2011). Tropical East African climate change and its relation to global climate: A record from Lake Tanganyika, Tropical East Africa, over the past 90+ kyr. Palaeogeography, Palaeoclimatology, Palaeoecology 303(1-4): 155-167.

Castañeda, I. S., J. P. Werne, et al. Organic geochemical records from Lake Malawi (East Africa) of the last 700 years, part II: Biomarker evidence for recent changes in primary productivity. Palaeogeography, Palaeoclimatology, Palaeoecology In Press, Corrected Proof.

Cerling, T. E., J. M. Harris, et al. (1997). Global vegetation change through the Miocene/Pliocene boundary. Nature 389(6647): 153-158.

Collister, J.W., Rieley, G., Stern, B., Eglinton, G., Fry, B., 1994. Compound-specific $\delta^{13}C$ analyses of leaf lipids from plants with differing carbon dioxide metabolisms. Organic Geochemistry 21 (6–7), 619–627.

Cranwell, 1985 P.A Cranwell, Long-chain unsaturated ketones in recent lacustrine sediments. Geochim. Cosmochim. Acta, 49 (1985), pp. 1545–1552.

Damsté, J. S. S., J. Ossebaar, et al. (2009). Fluxes and distribution of tetraether lipids in an equatorial African lake: Constraints on the application of the TEX_{86} palaeothermometer and BIT index in lacustrine settings. Geochimica et Cosmochimica Acta 73(14): 4232-4249.

Deines, P., 1980. The isotopic composition of reduced organic carbon. In: Fritz, P., Fontes, J.C. (Eds.), Handbook of Environmental Isotope Geochemistry. Elsevier, New York, pp. 329–406.

Dong J.S , Yongjin Wang, et al. (2010). A high-resolution stalagmite record of the Holocene East Asian monsoon from Mt Shennongjia, central China. The Holocene 20(2): 257-264.

Dykoski, C. A., R. L. Edwards, et al. (2005). A high-resolution, absolute-dated Holocene and deglacial Asian monsoon record from Dongge Cave, China. Earth and Planetary Science Letters 233(1-2): 71-86.

Eglinton, G., Hamilton, R.J., 1967. Leaf epicuticular waxes. Science 156, 1322–1334.

Erez J. and Luz B. (1983). Experimental paleotemperature equation for planktonic foraminifera. Geochim. Cosmochim. Acta 47, 1025–1031.

Fawcett, P. J., J. P. Werne, et al. (2011). Extended megadroughts in the southwestern United States during Pleistocene interglacials. Nature 470(7335): 518-521.

Feakins, S., Eglinton, T., deMenocal, P.B. A comparison of biomarker records of Northeast African vegetation from lacustrine and marine sediments ca. 3.4 Ma. Organic Geochemistry 38 (2007) 1607–1624.

Feng, Z. D., C. B. An, et al. (2006). Holocene climatic and environmental changes in the arid and semi-arid areas of China: a review. Holocene 16(1): 119-130.

Feng, Z. D., L. Y. Tang, et al. (2006). Holocene vegetation variations and the associated environmental changes in the western part of the Chinese Loess Plateau. Palaeogeography, Palaeoclimatology, Palaeoecology 241(3-4): 440-456.

Fontes, J.-C., Gasse, F., Gibert, E., 1996. Holocene environmental changes in Bangong Co Basin (Western Tibet): Part 1. Chronology and stable isotopes of carbonates of a Holocene lacustrine core. Palaeogeography, Palaeoclimatology,Palaeoecology 120, 25–47.

Freeman, K., and Colarusso, L., 2001, Molecular and isotopic records of C_4 grassland expansion in the late Miocene: Geochimica et Cosmochimica Acta, v. 65p. 1439-1454.

Galy, V., T. Eglinton, et al. (2011). The provenance of vegetation and environmental signatures encoded in vascular plant biomarkers carried by the Ganges–Brahmaputra rivers. Earth and Planetary Science Letters 304(1-2): 1-12.

Galy, V., L. François, et al. (2008). C_4 plants decline in the Himalayan basin since the Last Glacial Maximum. Quaternary Science Reviews 27(13-14): 1396-1409.

Gasse, F., Arnold, M., Fontes, J.-C., Fort, M., Gibert, E., Huc, A., Li, B., Li, Y., Liu, Q., Melieres, F., Van Campo, E., Wang, F., Zhan, Q., 1991. A 13,000 year climate record from western Tibet. Nature 353, 742– 745

Garzione, C. N., J. Quade, et al. (2000). Predicting paleoelevation of Tibet and the Himalaya from [delta]18O vs. altitude gradients in meteoric water across the Nepal Himalaya. Earth and Planetary Science Letters 183(1-2): 215-229.

Gupta, A. K., D. M. Anderson, et al. (2003). Abrupt changes in the Asian southwest monsoon during the Holocene and their links to the North Atlantic Ocean. Nature 421(6921n): 354-357.

Harris, N. (2006). The elevation history of the Tibetan Plateau and its implications for the Asian monsoon. Palaeogeography, Palaeoclimatology, Palaeoecology 241(1): 4-15.

He, Y., Theakstone, W.H., Zhang, Z., Zhang, D., Yao, T., Chen, T., Shen, Y., Pang, H., 2004. Asynchronous Holocene climatic change across China. Quaternary Research 61, 52– 63.

Henderson, A. C. G. and J. A. Holmes (2009). Palaeolimnological evidence for environmental change over the past millennium from Lake Qinghai sediments: A review and future research prospective. Quaternary International 194(1-2): 134-147.

Herzschuh, U., K. Winter, et al. (2006). A general cooling trend on the central Tibetan Plateau throughout the Holocene recorded by the Lake Zigetang pollen spectra. Quaternary International 154-155: 113-121.

Hopmans, E. C., J. W. H. Weijers, et al. (2004). A novel proxy for terrestrial organic matter in sediments based on branched and isoprenoid tetraether lipids. Earth and Planetary Science Letters 224(1-2): 107-116.

Hou, J., W. J. D'Andrea, et al. (2008). Can sedimentary leaf waxes record D/H ratios of continental precipitation? Field, model, and experimental assessments. Geochimica et Cosmochimica Acta 72(14): 3503-3517.

Hren, M. T., B. Bookhagen, et al. (2009). $\delta^{18}O$ and δD of streamwaters across the Himalaya and Tibetan Plateau: Implications for moisture sources and paleoelevation reconstructions. Earth and Planetary Science Letters 288(1-2): 20-32.

Huang, F. (2000). Vegetation and climate changes from 13 ka to 5 ka BP in Peiku Co, Tibet. Acta Palaeontologica Sinica , 39 (3): 441 - 448 (in Chinese)

Huang, Y., L. Dupont, et al. (2000). Mapping of C_4 plant input from North West Africa into North East Atlantic sediments. Geochimica et Cosmochimica Acta 64(20): 3505-3513.

Huang, Y., Street-Perrott, F.A., Metcalfe, S.E., Brenner, M., Moreland, M., Freeman, K.H., 2001. Climate change as the dominant control on glacial–interglacial variations in C_3 and C_4 plant abundance.Science 293, 1647–1651.

Huang Y., Shuman B., Wang Y. and Webb, III., T. (2002) Hydrogen isotope ratios of palmitic acid in lacustrine sedimentsrecord late Quaternary climate variations. Geology 30, 1103–1106.

Huang, Y., B. Shuman, et al. (2006). Climatic and environmental controls on the variation of C_3 and C_4 plant abundances in central Florida for the past 62,000 years. Palaeogeography, Palaeoclimatology, Palaeoecology 237(2-4): 428-435.

Hughen KA, Lehman S, Southon J, Overpeck J, Marchal O, Herring C, Turnbull J. 2004. C-14 activity and global carbon cycle changes over the past 50,000 years. Science 303 (5655): 202-207.

Huguet, A., C. Fosse, et al. (2010). Occurrence and distribution of glycerol dialkyl glycerol tetraethers in a French peat bog. Organic Geochemistry 41(6): 559-572.

Jin, Z., M. J. Bickle, et al. (2009). Early to mid-Pleistocene ostracod $\delta^{18}O$ and $\delta^{13}C$ in the central Tibetan Plateau: Implication for Indian monsoon change. Palaeogeography, Palaeoclimatology, Palaeoecology 280(3-4): 406-414.

Johnson, T. C., E. T. Brown, et al. (2011). Biogenic silica deposition in Lake Malawi, East Africa over the past 150,000 years. Palaeogeography, Palaeoclimatology, Palaeoecology 303(1-4): 103-109.

Kaiser, K., Z. Lai, et al. (2009). Stratigraphy and palaeoenvironmental implications of Pleistocene and Holocene aeolian sediments in the Lhasa area, southern Tibet (China). Palaeogeography, Palaeoclimatology, Palaeoecology 271(3-4): 329-342.

Kaiser, K., L. Opgenoorth, et al. (2009). Charcoal and fossil wood from palaeosols, sediments and artificial structures indicating Late Holocene woodland decline in southern Tibet (China). Quaternary Science Reviews 28(15-16): 1539-1554.

Kim, J.-H., J. van der Meer, et al. (2010). New indices and calibrations derived from the distribution of crenarchaeal isoprenoid tetraether lipids: Implications for past sea surface temperature reconstructions. Geochimica et Cosmochimica Acta 74(16): 4639-4654.

Lehmkuhl, F. and F. Haselein (2000). Quaternary paleoenvironmental change on the Tibetan Plateau and adjacent areas (Western China and Western Mongolia). Quaternary International 65-66: 121-145.

Lister, G.S., Kelts, K., Chen, K., Yu, J., Niessen, F. (1991) Lake Qinghai, China: closed-basin lake levels and the oxygen isotope record for ostracoda since the latest Pleistocene. Palaeogeography, Palaeoclimatology, Palaeoecology 84, 141– 162.

Liu, J., D.G. Martinson, X. Yuan, and D. Rind (2002) Evaluating Antarctic sea ice variability and its teleconnections in global climate models. Int. J. Climatology., 22, 885-900, doi:10.1002/joc.770.

Liu, D., Y. Wang, et al. (2008). A detailed comparison of Asian Monsoon intensity and Greenland temperature during the Allerød and Younger Dryas events. Earth and Planetary Science Letters 272(3-4): 691-697.

Liu, W. and Y. Huang (2005). Compound specific D/H ratios and molecular distributions of higher plant leaf waxes as novel paleoenvironmental indicators in the Chinese Loess Plateau. Organic Geochemistry 36(6): 851-860.

Liu, X., H. Dong, et al. (2009). Late Holocene forcing of the Asian winter and summer monsoon as evidenced by proxy records from the northern Qinghai-Tibetan Plateau. Earth and Planetary Science Letters 280(1-4): 276-284.

Loomis, S. E., J. M. Russell, et al. (2011). Distributions of branched GDGTs in soils and lake sediments from western Uganda: Implications for a lacustrine paleothermometer. Organic Geochemistry 42(7): 739-751.

Makou, M. C., K. A. Hughen, et al. (2007). Isotopic records of tropical vegetation and climate change from terrestrial vascular plant biomarkers preserved in Cariaco Basin sediments. Organic Geochemistry 38(10): 1680-1691.

Meyers, P.A., Eadie, B.J., 1993. Sources, degradation and recycling of organic matterassociated with sinking particles in Lake Michigan. Organic Geochemistry 20 (1), 47–56.

Meyers, P.A., 1997. Organic geochemical proxies of paleoceanographic, paleolimnologic, and paleoclimatic processes. Organic Geochemistry 27, 213–250.

Mingram, J., Schettler, G., Nowaczyk, N., Luo, X. J., Lu, H. Y., Liu, J. Q. & Negendank, J. F. W. (2004). A high-resolution record of palaeoenvironmental and palaeoclimatic changes over the last 78000 years from South China. Quaternary International 122, 85–107.

Mischke, S. and C. Zhang Holocene cold events on the Tibetan Plateau." Global and Planetary Change In Press, Corrected Proof.

Mischke, S. and C. Zhang (2010). Holocene cold events on the Tibetan Plateau. Global and Planetary Change 72(3): 155-163.

Morinaga, H., Itota, C., Isezaki, N., Goto, H., Yaskawa, K., Kusakabe, M., Liu, J., Gu, Z., Yuan, B. and Cong, S. (1993). Oxygen-18 and carbon-13 records for the last 14,000 years from Lacustrine carbonates of Siling-Co (lake) in the Qinghai-Tibetan Plateau. Geophysical Research Letters 20(24): doi: 10.1029/93GL02982. ISSN: 0094-8276.

Morrill, C. 2004. The influence of Asian monsoon variability on the water balance of a Tibetan lake. Journal of Paleolimnology 32: 273-286.

Morrill, C., J. T. Overpeck, et al. (2006). Holocene variations in the Asian monsoon inferred from the geochemistry of lake sediments in central Tibet. Quaternary Research 65(2): 232-243.

Nath, B. N., S. M. Gupta, et al. (2005). Evidence of Himalayan erosional event at ~0.5 Ma from a sediment core from the equatorial Indian Ocean in the vicinity of ODP Leg 116 sites. Deep Sea Research Part II: Topical Studies in Oceanography 52(14-15): 2061-2077.

Owen, L. A. (2009). Latest Pleistocene and Holocene glacier fluctuations in the Himalaya and Tibet. Quaternary Science Reviews 28(21-22): 2150-2164.

Pagani, M., Freeman, K.H., and Arthur, M.A., (1999), Late Miocene atmospheric CO_2 concentrations and the expansion of C_4 grasses, Science, 285, 876-879.

Pagani, M., Zachos, J., Freeman, K. H., Bohaty, S., and Tipple, B., (2005) Marked change in atmospheric carbon dioxide concentrations during the Oligocene, *Science*. 309, 600-603.

Pearson, E. J., S. Juggins, et al. (2011). A lacustrine GDGT-temperature calibration from the Scandinavian Arctic to Antarctic: Renewed potential for the application of GDGT-paleothermometry in lakes. Geochimica et Cosmochimica Acta 75(20): 6225-6238.

Peng, J., (1997), Ostracod assembaleges and environmental changes during 13,000 a BP and 4,500 a BP in Peiku Co, Tibet. Act a Micr opalaeontologica Sinica, 14(3) : 239- 254 (in Chinese)

Peterse, F., E. C. Hopmans, et al. (2011). Identification and distribution of intact polar branched tetraether lipids in peat and soil. Organic Geochemistry 42(9): 1007-1015.

Peterse, F., J.-H. Kim, et al. (2009). Constraints on the application of the MBT/CBT palaeothermometer at high latitude environments (Svalbard, Norway). Organic Geochemistry 40(6): 692-699.

Polissar, P. J. and K. H. Freeman. Effects of Aridity and Vegetation on Plant-wax δD in Modern Lake Sediments. Geochimica et Cosmochimica Acta In Press, Accepted Manuscript.

Polissar, P. J., K. H. Freeman, et al. (2009). Paleoaltimetry of the Tibetan Plateau from D/H ratios of lipid biomarkers. Earth and Planetary Science Letters 287(1-2): 64-76.

Powers, L.A., Werne, J.P., Johnson, T.C., Hopmans, E.C., Sinninghe Damsté, J.S., Schouten, S., 2004. Crenarchaeotal membrane lipids in lake sediments: a new paleotemperature proxy for continental\ paleoclimate reconstruction? Geology 32, 613–616.

Powers, L.A., Johnson, T.C., Werne, J.P., Castaneda, I.S., Hopmans, E.C., Sinninghe Damsté, J.S., Schouten, S., 2005. Large temperature variability in the southern African tropics since the last glacial maximum. Geophysical Research Letters 32, L08706.

Powers, L., J. P. Werne, et al. (2010). Applicability and calibration of the TEX_{86} paleothermometer in lakes. Organic Geochemistry 41(4): 404-413.

Reimer, P. J., M. G. L. Baillie, et al. (2004). IntCal04 terrestrial radiocarbon age calibration, 0-26 cal kyr BP. Radiocarbon 46(3): 1029-1058.

Rieley, G., et al., (1991). Sources of sedimentary lipids deduced from stable carbon isotope analyses of individual compounds. Nature 352 (6334), 425–427.

Rohling, E. J., Q. S. Liu, et al. (2009). Controls on the East Asian monsoon during the last glacial cycle, based on comparison between Hulu Cave and polar ice-core records. Quaternary Science Reviews 28(27-28): 3291-3302.

Ruddiman, W., Kutzbach, J., (1991). Plateau uplift and climatic change. Scientific America. 264, 66–75.

Rueda, G., A. Rosell-Melé, et al. (2009). Comparison of instrumental and GDGT-based estimates of sea surface and air temperatures from the Skagerrak. Organic Geochemistry 40(2): 287-291.

Sachse, D., J. Radke, et al. (2004). Hydrogen isotope ratios of recent lacustrine sedimentary n-alkanes record modern climate variability. Geochimica et Cosmochimica Acta 68(23): 4877-4889.

Sage, R. F. and S. A. Cowling (1999). 11 - Implications of Stress in Low CO_2 Atmospheres of the Past: Are Today's Plants Too Conservative for a High CO_2 World? Carbon Dioxide and Environmental Stress. L. Yiqi and A. M. Harold. San Diego, Academic Press: 289-308.

Schefuss, E., Schouten, S., Jansen, J.H.F., Sinninghe Damste, J.S. (2003). African vegetation controlled by tropical sea surface temperatures in the mid-Pleistocene period. Nature 422, 418–421

Schouten, S., Hopmans, E.C., Schefuß, E., Sinninghe Damste, J.S. (2002). Distributional variations in marine crenarchaeotal membrane lipids: a new organic proxy for reconstructing ancient sea water temperatures? Earth and Planetary Science Letters 204, 265–274.

Schouten, S., Huguet, C., Hopmans, E.C., Kienhuis, M.V.M., Sinninghe Damste, J.S., (2007). Improved analytical methodology and constraints on analysis of the TEX86 paleothermometer by high performance liquid chromatography/ atmospheric pressure chemical ionization-mass spectrometry. Analytical Chemistry 79, 2940–2944.

Shen, J., Liu, X.Q.,Wang, S.M., Matsumoto, R., (2005). Palaeoclimatic changes in the Qinghai\ Lake area during the last 18,000 years. Quaternary International 136, 131–140.

Sinninghe Damsté, J. S., J. Ossebaar, et al. (2008). Altitudinal shifts in the branched tetraether lipid distribution in soil from Mt. Kilimanjaro (Tanzania): Implications for the MBT/CBT continental palaeothermometer. Organic Geochemistry 39(8): 1072-1076.

Sluijs, A., S. Schouten, et al. (2006). Subtropical Arctic Ocean temperatures during the Palaeocene/Eocene thermal maximum. Nature 441(7093): 610-613.

Street-Perrott, F. A., K. J. Ficken, et al. (2004). Late Quaternary changes in carbon cycling on Mt. Kenya, East Africa: an overview of the $\delta^{13}C$ record in lacustrine organic matter. Quaternary Science Reviews 23(7-8): 861-879.

Thompson, L.G., Yao, T., Davis, M.E., Henderson, K.A., Mosley-Thompson, E., Lin, P.-N., Beer, J., Synal, H.-A., Cole-Dai, J., Bolzan, J.F., 1997.Tropical climate instability: the last glacial cycle from a Qinghai–Tibetan ice core. Science 276, 1821– 1825.

Tierney, J.E., Russell, J.M., Huang, Y., Sinninghe Damsté, J.S., Hopmans, E.C., Cohen, A.S., 2007. Northern Hemisphere controls on tropical Southeast African climate during the past 60,000 years. Science 322, 252–255.

Tierney, J. E. and J. M. Russell (2009). Distributions of branched GDGTs in a tropical lake system: Implications for lacustrine application of the MBT/CBT paleoproxy. Organic Geochemistry 40(9): 1032-1036.

Tierney, J. E., J. M. Russell, et al. Environmental controls on branched tetraether lipid distributions in tropical East African lake sediments. Geochimica et Cosmochimica Acta In Press, Corrected Proof.
Tierney, J. E., J. M. Russell, et al. (2010). A molecular perspective on Late Quaternary climate and vegetation change in the Lake Tanganyika basin, East Africa. Quaternary Science Reviews 29(5-6): 787-800.

Van Campo, E., Gasse, F., 1993. Pollen- and diatom-inferred climatic and hydrological changes in Sumxi Co Basin (western Tibet) since 13,000 yr B.P. Quaternary Research 39, 300– 313.

Wang, Y. J., H. Cheng, et al. (2001). A High-Resolution Absolute-Dated Late Pleistocene Monsoon Record from Hulu Cave, China. Science 294(5550): 2345-2348.

Wang, N., Yao, T., Thompson, L.G., Henderson, K.A., Davis, M.E., 2002. Evidence for cold events in the early Holocene from the Guliya icecore, Tibetan Plateau, China. Chinese Science Bulletin 47.17, 1422– 1427.

Wang, Y., H. Cheng, et al. (2005). The Holocene Asian Monsoon: Links to Solar Changes and North Atlantic Climate. Science 308(5723): 854-857.

Wang, Y., X. Liu, et al. (2010). Asynchronous evolution of the Indian and East Asian Summer Monsoon indicated by Holocene moisture patterns in monsoonal central Asia. Earth-Science Reviews 103(3-4): 135-153.

Wanner, H., O. Solomina, et al. (2011). Structure and origin of Holocene cold events. Quaternary Science Reviews 30(21-22): 3109-3123.

Watanabe, Y. W., Shigemitsu, M. and Tadokoro, T. (2008). Evidence of a change in oceanic fixed nitrogen with decadal climate change in the North Pacific subpolar region. *Geophys. Res. Lett.* 35, L01602, doi:10.1029/2007GL032188.

Watanabe, T., T. Matsunaka, et al. (2010). Last glacial-Holocene geochronology of sediment cores from a high-altitude Tibetan lake based on AMS 14C dating of plant fossils: Implications for paleoenvironmental reconstructions. Chemical Geology 277(1-2): 21-29.

Webster, P. 1994: The Role of Hydrological Processes in Ocean-Atmosphere Interaction. Rev. of Geophys., 32, 427-476.

Weijers, J. W. H., S. Schouten, et al. (2006). "Occurrence and distribution of tetraether membrane lipids in soils: Implications for the use of the TEX86 proxy and the BIT index." Organic Geochemistry 37(12): 1680-1693.

Weijers, J. W. H., S. Schouten, et al. (2007). Environmental controls on bacterial tetraether membrane lipid distribution in soils. Geochimica et Cosmochimica Acta 71(3): 703-713.

Weijers, J. W. H., S. Schouten, et al. (2004). Water table related variations in the abundance of intact archaeal membrane lipids in a Swedish peat bog. FEMS Microbiology Letters 239(1): 51-56.

Weninger, B. and O. Jöris (2008). A ^{14}C age calibration curve for the last 60 ka: the Greenland-Hulu U/Th timescale and its impact on understanding the Middle to Upper Paleolithic transition in Western Eurasia." Journal of Human Evolution 55(5): 772-781.

Wu, Y.H., Lücke, A., Jin, Z.D., Wang, S.M., Schleser, G., Battarbee, R.W., Xia, W.L., 2006. Holocene climate development on the central Tibetan Plateau: a sedimentary record from Cuoe Lake. Palaeogeography, Palaeoclimatology, Palaeoecology 234, 328–340.

Xie, S. and J. Guo(2004). Restricted utility of δ13C of bulk organic matter as a record of paleovegetation in some loess–paleosol sequences in the Chinese Loess Plateau. Quaternary Research 62(1): 86-93.

Yang, B., A. Braeuning, et al. (2007). Correlation between the oxygen isotope record from Dasuopu ice core and the Asian Southwest Monsoon during the last millennium. Quaternary Science Reviews 26(13-14): 1810-1817.

Yanhong, W., A. Lücke, et al. (2006). Holocene climate development on the central Tibetan Plateau: A sedimentary record from Cuoe Lake. Palaeogeography, Palaeoclimatology, Palaeoecology 234(2-4): 328-340.

Yao, T. and Shi, Y. 1992. Climatic changes of Holocene reflected in the ice core from Dunde, Qilian Mountains. In: Shi, Y. *et al.* (Eds). The Climates and Environments of Holocene Megathermal in China. China Ocean Press, Beijing, China, pp. 206-211.

Zhang, H. C., Y. Z. Ma, et al. (2000). A Holocene climatic record from arid northwestern China. Palaeogeography, Palaeoclimatology, Palaeoecology 162(3-4): 389-401.

Zhao, Y., Z. Yu, et al. Holocene vegetation and climate histories in the eastern Tibetan Plateau: controls by insolation-driven temperature or monsoon-derived precipitation changes? Quaternary Science Reviews In Press, Corrected Proof.

Zhu, L.P., Zhen, X.L., Wang, J.B., Lv, H.Y., Xie, M.P., Kitagawa, H., Possnert, G., 2009. A
30,000-year record of environmental changes inferred from Lake Chen Co, southern Tibet. Journal of Paleolimnology 42 (3), 343–358.

8. APPENDIX

Table 1 Total carbon (TC%) and total inorganic carbon (TIC%)

sample ID	depth (cm)	TIC %	TC %	TOC %	Duplicate TIC%	Duplicate TC%
1U-1-0	1	3.5729	4.1395	0.5666		
1U-1-15	15	3.6788	4.4209	0.7421	3.6901	
1U-1-29	30	3.7241	4.5149	0.7908		
1U-1-35	36	4.0104	4.8377	0.8273		
1U-1-45	45	3.9068	4.8670	0.9602	3.726	
1U-1-59	60	3.7993	4.5204	0.7211		
1U-1-75	75	3.8747	4.5953	0.7206	3.8134	
1U-1-80	81	4.1264	4.8118	0.6854		
1U-1-89	89	3.9868	4.5585	0.5717		
1U-1-105	105	3.8927	4.7818	0.8891	3.7752	
1U-1-119	120	4.1834	4.7618	0.5784		
1U-1-135	135	2.8593	3.5025	0.6432	2.971	
1U-2-6	150	3.5402	4.0058	0.4656		
1U-2-17	160	3.6622	4.2439	0.5817	3.5647	
1U-2-35	180	3.3745	3.7037	0.3292		
1U-2-47	190	3.3802	3.8126	0.4324	3.3884	
1U-2-55	200	3.2264	3.7022	0.4758		
1U-2-66	210	3.0068	3.3811	0.3743		
1U-2-77	220	4.1351	4.5961	0.461	4.2957	
1U-2-86	230	2.8411	3.1785	0.3374		
1U-2-96	240	2.4318	2.6564	0.2246		
1U-2-107	250	2.1653	2.5245	0.3592	2.2037	
1U-2-117	260	2.7758	3.2887	0.5129		
1U-2-126	270	2.2447	2.6609	0.4162	2.2258	2.669
1U-2-137	280	2.2965	2.7099	0.4134	2.2905	2.6576
2U-1-97	288	2.12	2.6576	0.5376	1.9872	
2U-1-102	295	2.4278	3.8776	1.4498		
2U-1-108	300	3.767	4.1962	0.4292		
2U-1-127	318	5.7945	6.2281	0.4336	6.0367	
2U-2-7	330	2.2368	2.5901	0.3533		
2U-2-17	340	1.6862	2.2030	0.5168	1.7502	
2U-2-37	360	2.165	2.3678	0.2028		
2U-2-47	370	1.8811	2.5402	0.6591	2.0438	
2U-2-67	390	2.2279	2.7154	0.4875		
2U-2-77	400	2.1318	2.9992	0.8674	2.1845	
2U-2-87	410	4.7859	5.5784	0.7925		
2U-2-97	420	4.6453	5.3130	0.6677		

Table 1 continued

sample ID	depth (cm)	TIC %	TC %	TOC %	dup TIC%	dup TC%
2U-2-107	430	3.7434	4.4124	0.669	3.8913	
2U-2-127	450	2.6631	4.6865	2.0234		
3U-1-69	480	4.2864	4.6577	0.3713		
3U-1-77	485	2.9941	3.7991	0.805	2.8515	
3U-1-98	508	2.5924	2.9904	0.398		
3U-1-107	515	3.6396	4.2765	0.6369	4.1409	
3U-1-117	526	3.1738	3.6116	0.4378		
3U-1-122	531	3.7864	4.2689	0.4825		
3U-1-127	536	3.9994	4.3446	0.3452		
3U-1-133	542	4.2181	4.9002	0.6821		
3U-1-137	545	5.0438	5.1230	0.0792	5.224	
3U-1-142	550	5.0495	5.1437	0.0942	5.2743	4.9379
3U-1-144	553	4.6288	4.7690	0.1402		4.6426

Table 2. Abundance and distribution of n-fatty acids and Average Chain Length of C_{24}-C_{30} homologues

sample ID	Depth (cm)	Average concentration (µg/g dry weight)														ACL[1]
		C14	C15	C16	C17	C18	C20	C22	C23	C24	C25	C26	C27	C28	C30	C24-C30
1U-1-0	1	0.06	0.03	0.49	0.04	0.27	0.06	0.17	0.13	1.50	0.57	0.06	0.06	0.09	0.02	24.6
1U-1-29	30	0.04	0.03	0.27	0.03	0.15	0.04	0.09	0.07	0.83	0.23	0.04	0.04	0.07	0.02	24.7
1U-1-35	36	0.08	0.05	1.07	0.00	0.54	0.10	0.28	0.18	2.06	1.17	0.11	0.11	0.14	0.05	24.7
1U-1-59	60	0.05	0.03	0.50	0.29	0.39	0.05	0.11	0.07	0.71	0.31	0.00	0.00	0.04	0.10	24.9
1U-1-80	81	0.00	0.00	0.49	0.00	0.25	0.04	0.08	0.07	0.76	0.44	0.24	0.24	0.02	0.00	25.0
1U-1-89	89	0.00	0.00	0.26	0.00	0.13	0.04	0.04	0.03	0.24	0.20	0.00	0.00	0.02	0.00	24.6
1U-1-119	120	0.00	0.00	0.22	0.00	0.11	0.03	0.08	0.08	0.66	0.42	0.03	0.03	0.00	0.00	24.5
1U-2-6	150	0.00	0.00	0.26	0.00	0.13	0.00	0.00	0.00	0.08	0.05	0.00	0.00	0.00	0.00	24.4
1U-2-35	180	0.00	0.00	0.08	0.00	0.04	0.00	0.00	0.00	0.02	0.01	0.00	0.00	0.00	0.00	24.3
1U-2-55	200	0.00	0.00	0.19	0.00	0.09	0.02	0.00	0.00	0.03	0.00	0.00	0.00	0.00	0.00	24.0
1U-2-66	210	0.00	0.00	0.81	0.00	0.41	0.00	0.00	0.01	0.07	0.10	0.00	0.00	0.00	0.00	24.6
1U-2-86	230	0.00	0.00	0.33	0.00	0.16	0.02	0.03	0.00	0.07	0.06	0.00	0.00	0.00	0.00	24.5
1U-2-96	240	0.00	0.00	0.44	0.00	0.22	0.00	0.02	0.00	0.05	0.06	0.01	0.01	0.00	0.00	24.8
1U-2-117	260	0.00	0.00	0.57	0.01	0.29	0.00	0.01	0.00	0.09	0.04	0.01	0.01	0.00	0.00	24.5
1U-2-126	270	0.00	0.00	0.29	0.00	0.14	0.00	0.03	0.02	0.05	0.04	0.00	0.00	0.00	0.00	24.4
2U-1-102	295	0.00	0.00	0.49	0.00	0.25	0.02	0.09	0.00	0.05	0.04	0.00	0.00	0.00	0.00	24.5
2U-1-108	300	0.00	0.00	0.17	0.00	0.08	0.02	0.03	0.02	0.07	0.05	0.00	0.00	0.00	0.00	24.4
2U-2-7	330	0.00	0.00	0.13	0.00	0.07	0.00	0.00	0.00	0.03	0.02	0.00	0.00	0.00	0.00	24.4
2U-2-37	360	0.00	0.00	0.14	0.00	0.07	0.00	0.01	0.00	0.04	0.02	0.00	0.00	0.00	0.00	24.4
2U-2-67	390	0.00	0.00	0.18	0.00	0.09	0.00	0.00	0.00	0.05	0.03	0.00	0.00	0.00	0.00	24.4
2U-2-87	410	0.00	0.00	0.20	0.00	0.10	0.00	0.05	0.03	0.29	0.17	0.00	0.00	0.00	0.00	24.4
2U-2-97	420	0.00	0.00	0.64	0.00	0.32	0.10	0.04	0.02	0.12	0.12	0.00	0.00	0.00	0.00	24.5
2U-2-127	450	0.03	0.03	0.59	0.00	0.30	0.00	0.00	0.00	0.08	0.08	0.01	0.01	0.00	0.00	24.7
3U-1-69	480	0.00	0.00	0.31	0.00	0.16	0.00	0.03	0.02	0.08	0.08	0.02	0.02	0.02	0.00	25.1
3U-1-98	508	0.00	0.00	0.26	0.00	0.13	0.00	0.02	0.00	0.05	0.04	0.00	0.00	0.00	0.00	24.4
3U-1-117	526	0.00	0.00	0.36	0.00	0.18	0.00	0.02	0.00	0.05	0.05	0.00	0.00	0.09	0.00	26.2
3U-1-122	531	0.00	0.00	0.27	0.00	0.13	0.00	0.00	0.00	0.03	0.03	0.00	0.00	0.00	0.00	24.5
3U-1-127	536	0.00	0.00	0.11	0.00	0.06	0.00	0.00	0.00	0.00	0.00	0.00	0.00	0.00	0.00	n/a[3]
3U-1-133	542	0.00	0.00	0.44	0.00	0.22	0.09	0.00	0.00	0.00	0.00	0.00	0.00	0.00	0.00	n/a
3U-1-144	553	0.00	0.00	0.09	0.00	0.04	0.00	0.00	0.00	0.00	0.00	0.00	0.00	0.00	0.00	n/a
Total		0.26	0.18	10.66	0.37	5.51	0.62	1.23	0.75	8.17	4.44	0.53	0.53	0.50	0.19	-
Average		0.01	0.01	0.36	0.01	0.18	0.02	0.04	0.03	0.27	0.15	0.02	0.02	0.02	0.01	24.6
Max		0.08	0.05	1.07	0.29	5.51	0.10	0.28	0.18	2.06	1.17	0.24	0.24	0.14	0.10	26.2
Min		0.00	0.00	0.08	0.00	0.04	0.00	0.00	0.00	0.00	0.00	0.00	0.00	0.00	0.00	24.0

1. Average Chain Length of C_{24}-C_{30} homologs is calculate by $ACL=\Sigma(X_i*i)/\Sigma X_i$, where i=24~30, X_i is the abundance
2. n/a indicates values are not computable due to missing compounds

Table 3. $\delta^{13}C$ of fatty acids $C_{16,}$ C_{18} and C_{24}, C_{26}

Sample ID	Depth (cm)	Cal age (yrs BP)	$\delta^{13}C$ n-alkanoic acid (‰)							
			C16	±	C18	±	C24	±	C26	±
1U-1-0	1	254.49	n/a	n/a	n/a	n/a	n/a	n/a	n/a	n/a
1U-1-29	30	1044.91	n/a	n/a	n/a	n/a	n/a	n/a	n/a	n/a
1U-1-35	36	1208.45	-29.20	0.02	-27.84	0.48	-26.00	0.88	n/a	n/a
1U-1-59	60	1862.59	-28.98	0.24	-26.93	0.02	-24.56	0.35	-25.38	0.21
1U-1-80	81	2434.97	-26.46	0.25	-24.60	0.48	-24.34	0.75	-25.87	1.31
1U-1-89	89	2653.01	-28.70	0.32	-24.58	0.37	-24.07	0.18	-25.86	0.03
1U-1-119	120	3497.95	-28.44	0.48	-24.52	0.89	-22.96	0.99	-25.12	0.87
1U-2-6	150	4315.63	-29.33	0.13	-29.00	0.09	-23.73	0.48	-26.00	0.66
1U-2-35	180	5133.31	-28.24	0.42	-26.39	0.64	-24.17	1.07	-27.17	2.43
1U-2-55	200	5678.43	-26.04	0.09	-22.79	0.13	-23.88	0.50	-26.39	1.43
1U-2-66	210	5950.99	-26.26	0.28	-23.56	0.30	-24.12	0.17	-27.00	2.80
1U-2-86	230	6496.11	-25.55	0.15	-22.84	0.10	-26.26	0.36	-28.15	0.68
1U-2-96	240	6768.67	-27.23	0.58	-25.55	0.68	-27.03	1.33	-27.63	1.92
1U-2-117	260	7313.79	-26.37	0.06	-24.50	0.02	-28.60	0.48	-29.31	0.58
1U-2-126	270	7586.35	-27.84	0.15	-23.43	0.13	-27.35	0.50	-27.78	0.42
2U-1-102	295	8267.75	-25.17	0.12	-25.35	0.06	-26.35	0.07	-27.00	1.53
2U-1-108	300	8404.03	-24.07	0.39	-23.29	0.59	-26.27	0.76	-28.39	0.94
2U-2-7	330	9221.71	-25.50	0.60	-23.49	0.64	-26.90	0.81	-29.29	2.80
2U-2-37	360	10039.39	-25.25	0.48	-23.91	0.21	-27.29	0.08	-32.24	0.07
2U-2-67	390	10857.07	-23.92	0.11	-22.22	0.15	-27.16	0.14	-28.35	1.76
2U-2-87	410	11402.19	-24.88	0.25	-22.51	0.05	-26.05	0.12	-27.27	0.10
2U-2-97	420	11674.75	-25.55	0.48	-22.87	0.13	-26.97	0.41	-28.88	0.34
2U-2-127	450	12492.43	-24.29	3.10	-22.16	2.00	-27.41	0.90	n/a	n/a
3U-1-69	480	13310.11	-23.57	0.76	-21.25	0.75	-28.21	1.35	-28.42	1.45
3U-1-98	508	14073.28	-22.27	0.31	-20.81	0.40	-26.25	0.52	-28.21	0.29
3U-1-117	526	14563.89	-22.63	0.72	-21.58	0.80	-25.21	1.34	-27.93	1.90
3U-1-122	531	14700.17	-23.96	0.03	-22.92	0.18	-25.10	1.96	-27.11	1.41
3U-1-127	536	14836.45	-23.31	0.07	-21.88	0.06	n/a[1]	n/a	n/a	n/a
3U-1-133	542	14999.98	-21.86	0.93	-20.94	0.87	n/a	n/a	n/a	n/a
3U-1-144	553	15299.80	-21.96	0.24	-20.73	0.04	n/a	n/a	n/a	n/a

1. n/a means data not available due to missing compounds

Table 4. Relative abundance of isoprenoid GDGT derived from both Euryarchaeota (Figure 2.3.2 I, II, III and IV) and Thaumarchaota (labeled ubiquitous), GDGT derived from Thaumarchaota only (Figure 2.3.2 V and V') (labeled aquatic) and branched GDGTs (Figure 2.3.2 VI, VII and VIII) (labeled soil-derived).

Sample ID	Depth (cm)	Cal age (yrs BP)	Relative abundance % aquatic	soil-derived	ubiquitous	BIT Index
1U-1-0	1	254.49	65.66	19.33	80.67	0.23
1U-1-29	30	1044.91	63.82	32.64	67.36	0.34
1U-1-35	36	1208.45	48.56	48.35	51.65	0.50
1U-1-59	60	1862.59	31.66	65.95	34.05	0.68
1U-1-80	81	2434.97	49.22	43.84	56.16	0.47
1U-1-89	89	2653.01	39.49	31.15	68.85	0.44
1U-1-119	120	3497.95	32.32	44.79	55.21	0.58
1U-2-6	150	4315.63	24.51	47.95	52.05	0.66
1U-2-35	180	5133.31	24.36	55.00	45.00	0.70
1U-2-55	200	5678.43	22.25	56.92	43.08	0.72
1U-2-66	210	5950.99	22.50	66.06	33.94	0.75
1U-2-86	230	6496.11	21.77	51.00	49.00	0.70
1U-2-96	240	6768.67	25.89	58.49	41.51	0.70
1U-2-117	260	7313.79	20.18	70.74	29.26	0.78
1U-2-126	270	7586.35	21.24	67.83	32.17	0.76
2U-1-102	295	8267.75	20.23	74.66	25.34	0.79
2U-1-108	300	8404.03	29.36	60.51	39.49	0.68
2U-2-7	330	9221.71	20.63	64.63	35.37	0.76
2U-2-37	360	10039.39	19.06	76.09	23.91	0.80
2U-2-67	390	10857.07	25.68	67.26	32.74	0.73
2U-2-87	410	11402.19	31.86	61.03	38.97	0.66
2U-2-97	420	11674.75	30.16	64.38	35.62	0.68
2U-2-127	450	12492.43	24.27	57.19	42.81	0.71
3U-1-69	480	13310.11	20.42	65.43	34.57	0.76
3U-1-98	508	14073.28	19.27	59.18	40.82	0.76
3U-1-117	526	14563.89	45.03	48.93	51.07	0.52
3U-1-122	531	14700.17	25.89	69.42	30.58	0.73
3U-1-127	536	14836.45	46.35	44.86	55.14	0.49
3U-1-133	542	14999.98	12.16	85.25	14.75	0.88
3U-1-144	553	15299.80	n/a[1]	n/a	n/a	n/a

1. n/a means compounds not detectable due to low concentrations

Note: All the XRF elemental data in digital format are archived in the ITRAX laboratory at Large Lakes Observatory

Table 5. GDGT concentration data (numbers in the table represent the integrated area)

sampleID	m/z 1302	m/z 1300	m/z 1298	m/z 1296	m/z 1292	m/z 1292'	m/z 1050	m/z 1048
1U-1-0	188985.5	289621.5	201870.4	46874	3158348	23826.7	588081.4	72378.7
1U-1-29	58968.2	122796.2	138536	44669.6	6522316	63939.4	2236125.2	581655.9
1U-1-35	35790.3	64438.5	74060.4	22087	3047022	33967.8	1960450.2	487472
1U-1-59	23872.4	42651.9	55502.2	16145.4	1808628	21612.3	2232514	594798.8
1U-1-80	149833.8	331354.2	414672.5	89638.3	6924518.5	62856.6	4177228.5	1435355.1
1U-1-89	1294861.6	1099521.2	698033.3	99357.9	4257681.5	35148.3	2089275	790100.2
1U-1-119	826477.1	782994.3	576733.3	81852.4	3160532.8	42450.5	3356641.5	733273.6
1U-2-6	390883.5	243331.8	151499.5	18550.1	707410.1	8310.4	1115624.3	154711.5
1U-2-35	249479.9	171335.8	114473.4	20031.5	644769.4	10769.1	1183290.5	146485
1U-2-55	543683.7	316954.7	212116.4	29719.2	1159924.8	17889.2	2389536	277376
1U-2-66	96534	86891.6	98685.4	16041.3	576610.5	9736.9	1369099.5	164979.2
1U-2-86	192746.4	88729.9	57826.1	8064.7	272859.7	4998.9	520233.4	60138.6
1U-2-96	65661.1	42652.7	42101	8638.4	258602.2	5149.4	452515.3	57678.4
1U-2-117	102643.5	81369.6	72100.1	15105.6	593177.8	10085.2	1663548.1	173686.8
1U-2-126	62084.1	57357.6	51070.2	8427.6	341604.4	5922.5	897992.6	82460.6
2U-1-102	36026.8	56454.1	68469.5	11810.7	672407.6	10737.4	2000519.6	221629.4
2U-1-108	95143	176908.1	184477.8	39387.9	1418609.9	20134.4	2282342.5	468369
2U-2-7	192168.6	163766.9	94016.2	15769.5	641831.8	10258	1618444.3	193421.5
2U-2-37	36375.7	40973.3	59846	11957.4	576652.6	8574.9	1859432.4	189350.2
2U-2-67	16570.1	21329.8	28708.6	5687.6	258261.4	4687.3	566782.2	90980.7
2U-2-87	48716.7	118972.1	136391	32590.4	1491206.5	17309.8	2252562.5	430688.7
2U-2-97	68253.6	88209.9	116003.8	22215.7	1609557	15539.2	2745711.5	342413.3
2U-2-127	75329.8	75780.5	60110.8	10167.6	284755.2	4893	542491.9	79377.8
3U-1-69	281394.2	231016.5	187841.6	30834.7	1041346.4	13742.1	2666578.8	389465.2
3U-1-98	170762.5	128063.1	57508	8445.5	321675.2	4558.2	810784.6	83999.9
3U-1-117	12916.7	36636.5	62859.9	17705.6	957647.3	12496.6	683905.2	356689.1
3U-1-122	30344.7	46326.6	38395.8	8237.8	673507.1	7740.4	1008221.5	341864.8
3U-1-127	6737.4	11589.8	8736.6	2193.1	152932.5	1403.9	88598.9	20556.8
3U-1-133	1736.9	2055.3	2158.8	1217	33400	-	113986	18573.8
3U-1-144	-	-	-	-	2833.2	-	1687.2	-

Table 5 continued

sample id	m/z 1046	m/z 1036	m/z 1034	m/z 1032	m/z 1022	m/z 1020	m/z 1018
1U-1-0	207733.6	280578.4	304929.1	55200.6	68248.7	23074.4	10525.1
1U-1-29	781030.6	951183.6	1102391.4	654319.8	181071	56460	35395.2
1U-1-35	522842	900634.7	847982.4	512184.9	206540.8	28559.1	29462.2
1U-1-59	643794.8	1405661	860927.5	381634.1	174146.7	70776.3	22036.6
1U-1-80	1832438.5	1648671.1	2176599.3	995195.4	398593.5	164846.2	59964.1
1U-1-89	893124.4	1094738.2	1058150	506174.4	201669.9	82654.6	30593.8
1U-1-119	756226.6	834581.8	995248	429803	247865.3	81783.9	20446.4
1U-2-6	107491.5	218313.5	185703.7	65276.3	66268.2	18407.9	5408.5
1U-2-35	83292.4	223363.9	138482.4	39819.2	73490	17938.2	5832.2
1U-2-55	145638.3	479999.7	252709.1	63706.1	143541.1	31741.8	11700.9
1U-2-66	79102.7	262740.2	128603.3	32964.3	89754	20656.8	6741.8
1U-2-86	26879.7	99356.2	46883.3	10512.8	31285.1	6026.8	2146.6
1U-2-96	16051.9	108725.6	47357.3	9789.5	34550.4	9247.8	2998.9
1U-2-117	67465.2	337884.1	155913.3	32205.3	113107.5	23178.3	7702.4
1U-2-126	29152.5	161328.3	69895.5	14473.6	50493.9	11066.8	3462.8
2U-1-102	100385	389744.8	212014.7	42829.8	131008.2	32045.7	10847.8
2U-1-108	329320.8	528943.9	486893.1	193985.5	153723.8	41788.1	83897.3
2U-2-7	101761.8	322260.6	172154.9	35358.3	101807.8	22006.6	7478.7
2U-2-37	69895.5	370124	157866.8	31639.9	107217.9	22152.4	9435.5
2U-2-67	45904.7	100090.2	55200.6	14552.3	21994.9	6174.5	2663.4
2U-2-87	271207.7	507255.9	453029.2	153586.1	129523.9	41086.6	12314.1
2U-2-97	270323	571660.8	401732.1	145117.6	151702.9	45538.1	17927.1
2U-2-127	49124.3	112391.7	82532	26129.4	27688	110123	2660
3U-1-69	219554.8	562179.1	405010.1	132564.8	151791.5	38814.5	12581.2
3U-1-98	29726.1	146682.8	70683.7	13124.3	44286.1	12445.9	4413.7
3U-1-117	336892.2	230170.4	620931.9	365153.6	140248.2	115272.2	80494.2
3U-1-122	247765.3	575612.6	827839.6	289237.6	243010.3	151454.4	84399.5
3U-1-127	11298.1	46153.3	30560.3	10556	14629.1	3459.8	1736.2
3U-1-133	7930	88134.9	29044.4	7682.2	33213.6	5026.3	1069.3
3U-1-144	-	-	-	-	-	-	-

Note: the original GDGT concentration data are archived at Department of Geological Sciences, Brown University. A digital copy is also accessible at Large Lakes Observatory